

Ultra-luminous X-ray sources and remnants of massive metal-poor stars

M. Mapelli^{1,2}, E. Ripamonti², L. Zampieri³, M. Colpi², A. Bressan^{3,4}

¹ *Institute for Theoretical Physics, University of Zürich, Winterthurerstrasse 190, CH-8057, Zürich, Switzerland*

² *Università Milano Bicocca, Dipartimento di Fisica G. Occhialini, Piazza della Scienza 3, I-20126, Milano, Italy; mapelli@mib.infn.it*

³ *INAF-Osservatorio astronomico di Padova, Vicolo dell'Osservatorio 5, I-35122, Padova, Italy*

⁴ *Scuola Internazionale Superiore di Studi Avanzati (SISSA), via Beirut 4, I-34014, Trieste, Italy*

7 November 2018

ABSTRACT

Massive metal-poor stars might form massive stellar black holes (BHs), with mass $25 \leq m_{\text{BH}}/M_{\odot} \leq 80$, via direct collapse. We derive the number of massive BHs (N_{BH}) that are expected to form per galaxy through this mechanism. Such massive BHs might power most of the observed ultra-luminous X-ray sources (ULXs). We select a sample of 64 galaxies with X-ray coverage, measurements of the star formation rate (SFR) and of the metallicity. We find that N_{BH} correlates with the number of observed ULXs per galaxy (N_{ULX}) in this sample. We discuss the dependence of our model on the SFR and on the metallicity. The SFR is found to be crucial, consistently with previous studies. The metallicity plays a role in our model, since a lower metallicity enhances the formation of massive BHs. Consistently with our model, the data indicate that there might be an anticorrelation between N_{ULX} , normalized to the SFR, and the metallicity. A larger and more homogeneous sample of metallicity measurements is required, in order to confirm our results.

Key words: black hole physics – X-rays: binaries – X-rays: galaxies – galaxies: starburst

1 INTRODUCTION

Ultra-luminous X-ray sources (ULXs, see Mushotzky 2004 for a review, and references therein) are defined as non-nuclear point-like sources with isotropic X-ray luminosity $L_X \gtrsim 10^{39} \text{ erg s}^{-1}$. The mechanism that powers the ULXs is still unknown, although various scenarios have been proposed. ULXs could be associated with high-mass X-ray binaries (HMXBs) powered by stellar-mass black holes (BHs) with anisotropic X-ray emission (e.g. King et al. 2001) or with super-Eddington accretion rate/luminosity (e.g. Begelman 2002; King & Pounds 2003; Socrates & Davis 2006; Poutanen et al. 2007) or with a combination of the two mechanisms (e.g. King 2008). ULXs could also be associated with HMXBs powered by intermediate-mass BHs (IMBHs), i.e. BHs with mass $100 M_{\odot} \leq m_{\text{BH}} \leq 10^5 M_{\odot}$ (see van der Marel 2004 for a review). IMBHs with mass larger than $100 M_{\odot}$ may be required to explain the brightest ULXs (i.e. the $\lesssim 4$ ULXs with $L_X \gtrsim 10^{41} \text{ erg s}^{-1}$), those ULXs showing quasi-periodic oscillations (M82 X-1, see Strohmayer & Mushotzky 2003, and NGC 5408 X-1, see Strohmayer et al. 2007) and some of those that are surrounded by isotropically ionized nebulae (Pakull & Mirioni 2002; Kaaret, Ward & Zezas 2004). However, IMBHs are not needed to explain the observational properties of most of the ULXs (e.g. Gonçalves

& Soria 2006; Stobbs, Roberts & Wilms 2006; Copperwheat et al. 2007; Roberts 2007; Zampieri & Roberts 2009). Thus, the objects classified as ULXs might actually be an inhomogeneous sample, including sources of different nature.

Most of ULXs are located in galaxies with a high star formation rate (SFR, e.g. Irwin, Bregman & Athey 2004), although a small fraction (10–20 per cent, especially in the low-luminosity tail) might be associated with an old population (e.g. Colbert et al. 2004; Brassington, Read & Ponman 2005). The ULXs match the correlation between X-ray luminosity and SFR reported by various studies (Grimm, Gilfanov & Sunyaev 2003; Ranalli, Comastri & Setti 2003; Gilfanov, Grimm & Sunyaev 2004a,b,c; Kaaret & Alonso-Herrero 2008). Furthermore, the same studies indicate that the luminosity function of ULXs is the direct extension of that of HMXBs. Recent papers suggest a correlation between ULXs and low-metallicity environments, and propose that this may be connected with the influence of metallicity on the evolution of massive stars (Pakull & Mirioni 2002; Zampieri et al. 2004; Soria et al. 2005; Swartz, Soria & Tennant 2008). This scenario has been explored in detail by Mapelli, Colpi & Zampieri (2009, hereafter Paper I) and by Zampieri & Roberts (2009), highlighting that a large fraction of ULXs may actually host massive ($\sim 30 - 80 M_{\odot}$)

stellar BHs formed in a low-metallicity environment. In fact, low-metallicity massive ($\gtrsim 40 M_\odot$) stars lose only a small fraction of their mass due to stellar winds (Maeder 1992, hereafter M92; Heger & Woosley 2002, hereafter HW02; Heger et al. 2003, hereafter H03; Belczynski et al. 2010, hereafter B10) and can directly collapse (Fryer 1999; B10) into massive BHs ($25 M_\odot \leq m_{\text{BH}} \leq 80 M_\odot$). Such massive BHs can power most of the known ULXs without requiring super-Eddington accretion or anisotropic emission. Furthermore, their formation mechanism can explain the correlation between ULXs and SFR, and the fact that ULXs are preferentially found in low-metallicity regions. In this Paper, we extend to a larger sample of galaxies the analysis reported in Paper I, and we study the formation of massive BHs from the direct collapse of massive metal-poor stars and their possible connection with ULXs. In particular, we show that there is a correlation between the number of massive BHs formed in this scenario and the number of observed ULXs per galaxy.

2 METHOD

The aim of this Paper is to compute the number of massive BHs that are expected to form in a galaxy (N_{BH}) through the direct collapse of massive metal-poor stars. We will then compare such number with the observed number of ULXs (N_{ULX}) in the same galaxy and with other observational quantities (e.g. the SFR, the metallicity, etc.). In this Section, we start describing the procedure adopted for deriving N_{BH} and then present the properties of the galaxy sample used for the comparison.

2.1 The number of massive BHs

According to numerical models (Fryer 1999; HW02; H03), a star that, at the end of its life, has a final mass $m_{\text{fin}} \geq 40 M_\odot$ is expected to directly collapse into a BH. In this case, the mass of the remnant BH is likely more than half of the final mass of the progenitor star, as relatively small mass ejection is expected in the direct collapse. Thus, stars that at the end of their lives have $m_{\text{fin}} \geq 40 M_\odot$ are likely to produce massive BHs (B10).

The final masses of the stars strongly depend on their metallicity. Massive stars with metallicity close to solar cannot have final masses larger than $m_{\text{fin}} \sim 10 - 15 M_\odot$, even if their initial mass was very large, as they are expected to lose a lot of mass due to stellar winds (H03). Instead, massive stars with lower metallicity are less affected by stellar winds, and retain a larger fraction of their initial mass. If its metallicity is sufficiently low, a star can have a final mass $m_{\text{fin}} \geq 40 M_\odot$ and can directly collapse into a massive BH with a mass $25 M_\odot \leq m_{\text{BH}} \leq 80 M_\odot$ (HW02; H03; B10).

Thus, in order to compute the number of massive BHs N_{BH} , we first need to know for which metallicities massive stars can directly collapse into BHs. Evolutionary tracks of massive stars have been computed under different assumptions concerning the mass-loss rate (M92; Bressan et al 1993; Fagotto et al 1994a,b; Eldridge & Tout 2004; Eldridge & Vink 2006; B10), and thus predict different final stellar masses (differences are up to a factor of 2). In Paper I, we used the results from M92, that can be regarded as upper

limits. In this Paper, we base our calculations on the results of two previous studies: one relies on the PADOVA tracks (as described in Portinari, Chiosi & Bressan 1998, hereafter referred to as P98) and the other is presented by B10. P98 assume that all massive stars explode as supernovae, and do not consider the direct collapse scenario. Here, we follow the more recent studies by Fryer (1999) and by H03, indicating that, above $40 M_\odot$, the stars collapse to a massive BH. Thus, in the case of P98, we take the final stellar masses for various metallicities listed in their table 1, and we assume that all stars with $m_{\text{fin}} \geq 40 M_\odot$ end up into a massive BH¹.

Instead, B10 already include in their code the hypothesis that massive stars directly collapse into massive BHs. Thus, when we apply the results from B10 to our model, we consider the stars that end into BHs with $m_{\text{BH}} \gtrsim 25 M_\odot$ as progenitors of massive BHs (see fig. 1 of B10). This condition is approximately equivalent² to requiring that $m_{\text{fin}} \geq 40 M_\odot$.

Given these assumptions, we can derive the expected number of massive BHs per galaxy (N_{BH}) as a function of the star formation rate (SFR) and of the metallicity Z (see Paper I):

$$N_{\text{BH}}(\text{SFR}, Z) = A(\text{SFR}) \int_{m_{\text{prog}}(Z)}^{m_{\text{max}}} m^{-\alpha} dm, \quad (1)$$

where m_{max} is the maximum stellar mass (we assume $m_{\text{max}} = 120 M_\odot$) and α is the slope of the initial mass function (IMF). $m_{\text{prog}}(Z)$ is the minimum initial stellar mass (i.e. the mass at zero-age main sequence) for which a star is the progenitor of a massive BH. As we discussed above, $m_{\text{prog}}(Z)$ strongly depends on the metallicity. In our calculations, we assume $m_{\text{prog}}(Z)$ to be the initial stellar mass for which $m_{\text{fin}} \geq 40 M_\odot$ and $m_{\text{BH}} \gtrsim 25 M_\odot$, when adopting the models by P98 and by B10, respectively. Finally, $A(\text{SFR})$, the normalization constant in equation (1), can be estimated as

$$A(\text{SFR}) = \frac{\int_0^{t_{\text{SFR}}} \text{SFR}(t) dt}{\int_{m_{\text{min}}}^{m_{\text{max}}} m^{1-\alpha} dm}, \quad (2)$$

where m_{min} is the minimum stellar mass (we assume $m_{\text{min}} = 0.08 M_\odot$), $\text{SFR}(t)$ is the star formation rate as a function of time and t_{SFR} is the duration of the star formation.

¹ An important difference from the original assumptions made by P98 concerns the fate of very massive stars, with Hydrogen exhausted core at the end of the hydrostatic evolution, M_{He} , larger than $40 M_\odot$. For $M_{\text{He}} > 40 M_\odot$, P98 adopted the pair instability (Woosley & Weaver 1986) model with the following fates: for M_{He} in the range 40 to $60 M_\odot$ the star undergoes a pulsational instability leading to a final iron core collapse; in the range $M_{\text{He}} \sim 60$ to $\sim 100 M_\odot$ the star was supposed to undergo a complete disruption and finally, for even larger cores, a direct collapse to a BH.

² We assume $m_{\text{BH}} \gtrsim 25 M_\odot$ for B10, because the models (e.g. HW02; H03) show that in the direct collapse slightly more than half of the final mass of the star goes into the BH. As the minimum final stellar mass for direct collapse is $m_{\text{fin}} \geq 40 M_\odot$, $m_{\text{BH}} \gtrsim 20 - 30 M_\odot$ is a reasonable choice. On the basis of this argument, threshold masses anywhere in between 20 and $30 M_\odot$ would be fine. We choose $m_{\text{BH}} \gtrsim 25 M_\odot$ as a reasonable fiducial value. Furthermore, BHs with $m_{\text{BH}} \gtrsim 25 M_\odot$ are above the observed mass-range for stellar BHs ($3 - 20 M_\odot$, Orosz 2003).

However, we are not interested in all the massive BHs, but only in those that could acquire massive stellar companions and power observable ULXs. Thus, in the case of interest, equation (2) might be written as

$$A(\text{SFR}) = \frac{\text{SFR } t_{\text{co}}}{\int_{m_{\text{min}}}^{m_{\text{max}}} m^{1-\alpha} dm}, \quad (3)$$

where SFR is the current star formation rate and t_{co} is the characteristic lifetime of the companion of the massive BH. In this Paper, we adopt a constant value $t_{\text{co}} = 10^7$ yr. Such value is the lifetime of a $\sim 15 M_{\odot}$ star. In fact, according to theoretical models, massive BHs can power persistent ULXs only when their companion is sufficiently massive ($\geq 15 M_{\odot}$, Patruno et al. 2005). If the companion star is relatively low-mass ($2 \leq m/M_{\odot} < 10$), then the system can power only a transient ULX, with an outburst phase of a few days every few months³ (Portegies Zwart, Dewi & Maccarone 2004). The probability of observing such transient ULXs is a factor of $\gtrsim 10^2$ lower than the probability of observing persistent ULXs. Thus, the value of N_{BH} derived assuming $t_{\text{co}} = 10^7$ yr is not the total number of massive BHs present in a galaxy, but the number of massive BHs that could easily find a massive companion to accrete from.

Fig. 1 shows N_{BH} , normalized to the SFR, as a function of Z , for P98 and for B10. In this Fig., we adopt two different IMFs: (i) the Salpeter IMF (Salpeter 1955), for which $\alpha = 2.35$, and (ii) the Kroupa IMF, for which $\alpha = 1.3$ if $m \leq 0.5 M_{\odot}$ and $\alpha = 2.3$ for larger masses (Kroupa 2001). Fig. 1 indicates that N_{BH} has approximately the same trend when adopting the Salpeter or the Kroupa IMF, although the normalization is different by a factor of ~ 2 . In the following, we will consider, as reference, only the Kroupa IMF. As shown in Appendix A, where a more detailed comparison is reported, the results can be easily scaled to the Salpeter IMF. Fig. 1 shows also that the trend obtained adopting P98 is quite similar to the one obtained adopting B10. The main differences are in the normalization, as N_{BH} is a factor of $\sim 1.3 - 2.0$ lower for P98 than for B10, and in the cut-off, as N_{BH} goes to zero for $Z \sim 0.4 Z_{\odot}$ and $0.5 Z_{\odot}$ for P98 and B10, respectively.

Once N_{BH} is known, we can estimate the upper limit (ϵ_{BH}) of the fraction of massive BHs that power ULXs in a given galaxy at present, assuming that all the observed ULXs in this galaxy, corrected for the contamination (N_{ULX} , see next Section), are powered by a massive BH:

$$\epsilon_{\text{BH}} = \frac{N_{\text{ULX}}}{N_{\text{BH}}}. \quad (4)$$

2.2 The sample of galaxies

In order to compare the value of N_{BH} computed from equation (1) with the observed number of ULXs per galaxy (N_{ULX}), we selected a sample of galaxies (Table 1 and references in Appendix B) that satisfy the following criteria. (i)

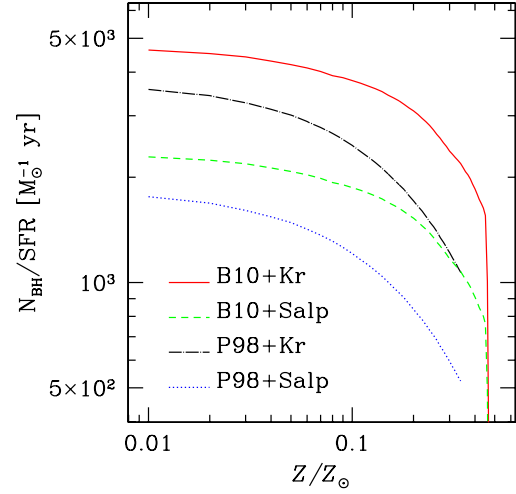


Figure 1. Number of expected massive BHs per galaxy, normalized to the SFR, as a function of Z . Solid line (red on the web): B10 with the Kroupa IMF; dashed line (green on the web): B10 with the Salpeter IMF; dot-dashed line (black): P98 with the Kroupa IMF; dotted line (blue on the web): P98 with the Salpeter IMF.

There exist X-ray observation(s) deep enough to detect the presence of ULXs. (ii) The selected galaxies have at least one measurement of the SFR. (iii) They have a sufficiently accurate measurement of the metallicity Z (in most cases even of the metallicity gradient). (iv) They are not elliptical galaxies.

The last criterion indicates that the galaxies in Table 1 are spiral, irregular or peculiar galaxies, but not elliptical galaxies. We decided not to include any elliptical galaxy in our sample, as ULXs in elliptical galaxies show properties that are quite different from those of ULXs in other galaxies, which may indicate a different origin for them (Swartz et al. 2004; Liu, Bregman & Irwin 2006; Winter, Mushotzky & Reynolds 2006). Furthermore, we remind that in early-type galaxies there is neither evidence of the presence of core-collapse supernovae nor of a significant fraction of massive star population, apart from small rejuvenation episodes (e.g. NGC 205, Bertola et al. 1995). ULXs in elliptical galaxies might be connected to the minor (but non-negligible) fraction of ULXs that is claimed (e.g. Colbert et al. 2004; Brasington et al. 2005) to be associated with old stellar populations (hereafter, we refer to them as Population II ULXs). Since old populations are present also in spiral galaxies, our sample may be contaminated by Population II ULXs. It is quite difficult to estimate their number, but it is reasonable to neglect their contribution in our sample (see Appendix B for details).

No complete catalogue of galaxies with and without ULXs exists. The most known available catalogues are Liu & Mirabel (2005; hereafter LM05) and Liu & Bregman (2005; hereafter LB05). LM05 is a catalogue of ULXs reported in the literature until April 2004. It does not include galaxies without ULXs, and it is quite non-uniform, as it reports observations with various instruments. LB05 is a catalogue of all the 313 nearby galaxies that have been observed with the

³ However, the Galactic transient source GRS 1915 + 105, which is associated to a low-mass X-ray binary system including a quite massive BH ($m_{\text{BH}} = 14.0 \pm 4.4 M_{\odot}$, Harlaftis & Greiner 2004), has a much longer outburst phase (> 17 years, see e.g. Castro-Tirado, Brandt & Lund 1992; Fender & Belloni 2004; Deegan, Combet & Wynn 2009), in partial contradiction with this model.

Table 1. Properties of the galaxies in our sample.

Galaxy	SFR ($M_{\odot} \text{ yr}^{-1}$)	Z (Z_{\odot})	$N_{\text{ULX, raw}}^{\text{a}}$	D (Mpc) ^b	Q ^c	$N_{\text{ULX}}^{\text{d}}$
The Cartwheel	20	0.14	19	124	0	$19.00^{+5.43}_{-4.32}$
NGC 253	4.0	0.24	3	3.0	$0.02^{+0.04}_{-0.01}$	$2.98^{+2.91}_{-1.63}$
NGC 300	0.14	0.19	0	2.02	0	$0.00^{+1.83}_{-0.00}$
NGC 598 (M 33)	1.1	0.32	1	0.92	$0.00^{+0.00}_{-0.00}$	$1.00^{+2.29}_{-0.83}$
NGC 628 (M 74)	2.2	0.27	2	8.5	$0.15^{+0.11}_{-0.06}$	$1.85^{+2.63}_{-1.29}$
NGC 1058	0.27	0.26	1	9.85	$0.09^{+0.06}_{-0.03}$	$0.91^{+2.29}_{-0.83}$
NGC 1073	1.2	0.34	2	15.2	0	$2.00^{+2.63}_{-1.29}$
NGC 1291	0.94	0.06	3	8.6	$0.16^{+0.11}_{-0.07}$	$2.84^{+2.91}_{-1.63}$
NGC 1313	1.4	0.1	2	3.7	0	$2.00^{+2.63}_{-1.29}$
NGC 1365	7.2	0.20	13	17.4	$0.82^{+0.20}_{-0.16}$	$12.18^{+4.70}_{-3.56}$
IC 342	0.48	0.19	2	3.9	$0.02^{+0.04}_{-0.01}$	$1.98^{+2.63}_{-1.29}$
NGC 1566	3.2	0.33	4	13.4	$1.50^{+0.18}_{-0.13}$	$2.50^{+3.16}_{-1.92}$
NGC 1705	0.087	0.19	0	6.0	0	$0.00^{+1.83}_{-0.00}$
NGC 2366	0.075	0.10	0	2.7	0	$0.00^{+1.83}_{-0.00}$
NGC 2403	0.4	0.22	1	3.1	0	$1.00^{+2.29}_{-0.83}$
NGC 2442	4.6	0.45	2	17.1	$1.33^{+0.10}_{-0.31}$	$0.67^{+2.65}_{-0.67}$
Holmberg II (Arp 268)	0.1	0.1	1	4.5	0	$1.00^{+2.29}_{-0.83}$
NGC 2903	1.9	0.28	2	7.4	$0.09^{+0.07}_{-0.04}$	$1.91^{+2.63}_{-1.29}$
NGC 3031 (M 81)	3.3	0.29	2	3.4	$0.03^{+0.05}_{-0.02}$	$1.97^{+2.63}_{-1.29}$
NGC 3049	0.57	0.60	0	19.9	0	$0.00^{+1.83}_{-0.00}$
PGC 30819 (IC 2574, UGC 05666)	0.057	0.17	0	3.5	0	$0.00^{+1.83}_{-0.00}$
NGC 3310 (Arp 217)	2.2	0.22	3	18.7	$0.16^{+0.03}_{-0.03}$	$2.84^{+2.91}_{-1.63}$
NGC 3395/3396 (Arp 270)	4.7	0.21	7	24.6	0	$7.00^{+3.76}_{-2.58}$
PGC 35286 (UGC 06456)	0.017	0.062	0	1.4	0	$0.00^{+1.83}_{-0.00}$
PGC 35684 (UGC 06541, Mkn 178)	0.01	0.091	0	4.0	0	$0.00^{+1.83}_{-0.00}$
NGC 3738 (Arp 234)	0.038	0.20	0	4.3	0	$0.00^{+1.83}_{-0.00}$
NGC 3972	0.30	0.35	0	17.0	0	$0.00^{+1.83}_{-0.00}$
Antennae (NGC 4038/4039, Arp 244)	7.1	0.04	15	21.5	0	$15.00^{+4.95}_{-3.83}$
NGC 4144	0.05	0.20	0	5.7	0	$0.00^{+1.83}_{-0.00}$
NGC 4214	0.13	0.21	0	3.5	0	$0.00^{+1.83}_{-0.00}$
NGC 4236	0.12	0.22	0	2.2	0	$0.00^{+1.83}_{-0.00}$
NGC 4248	0.018	0.26	0	7.3	0	$0.00^{+1.83}_{-0.00}$
NGC 4254 (M 99)	4.0	0.26	3	16.8	$1.39^{+0.11}_{-0.13}$	$1.61^{+2.91}_{-1.61}$
NGC 4258 (M 106)	2.5	0.32	3	7.7	$0.58^{+0.45}_{-0.25}$	$2.42^{+2.92}_{-1.69}$
NGC 4303 (M 61)	5.8	0.20	6	15.2	$1.91^{+0.58}_{-0.45}$	$4.09^{+3.60}_{-2.45}$
NGC 4321 (M 100)	4.8	0.28	7	14.1	$1.88^{+0.65}_{-0.49}$	$5.12^{+3.79}_{-2.66}$
NGC 4395	0.12	0.22	1	3.6	$0.04^{+0.07}_{-0.03}$	$0.96^{+2.29}_{-0.83}$
NGC 4449	0.28	0.25	0	3.0	0	$0.00^{+1.83}_{-0.00}$
NGC 4485/4490 (Arp 269)	4.5	0.23	5	8.55	$0.16^{+0.11}_{-0.06}$	$4.84^{+3.38}_{-2.16}$
NGC 4501 (M 88) ^e	3.5	0.49	2	16.8	$0.43^{+0.11}_{-0.09}$	$1.57^{+2.63}_{-1.29}$
NGC 4559	1.3	0.19	2	5.8	0	$2.00^{+2.63}_{-1.29}$
NGC 4631 (Arp 281)	2.80	0.22	2	6.9	$0.16^{+0.14}_{-0.08}$	$1.84^{+2.63}_{-1.30}$
NGC 4651 (Arp 189)	1.40	0.23	1	16.8	$0.17^{+0.04}_{-0.03}$	$0.83^{+2.29}_{-0.83}$
NGC 4656	0.95	0.075	1	7.2	$0.05^{+0.04}_{-0.02}$	$0.95^{+2.29}_{-0.83}$
The Mice (NGC 4676, Arp 242)	6.0	0.3	6	90.4	0	$6.00^{+3.58}_{-2.37}$
NGC 4736 (M 94)	1.1	0.20	1	5.2	$0.15^{+0.17}_{-0.08}$	$0.85^{+2.29}_{-0.85}$
NGC 4861 (Arp 266)	0.59	0.13	2	17.8	$0.11^{+0.03}_{-0.02}$	$1.89^{+2.63}_{-1.29}$
PGC 45561 (UGC 08231)	0.29	0.40	0	33.0	0	$0.00^{+1.83}_{-0.00}$
NGC 5033	1.50	0.069	2	15.2	$0.69^{+0.21}_{-0.16}$	$1.31^{+2.63}_{-1.30}$
NGC 5055 (M 63)	1.70	0.30	2	8.5	$0.18^{+0.13}_{-0.07}$	$1.82^{+2.63}_{-1.29}$
NGC 5194/5195 (M 51, Arp 85)	13.0	0.39	9	7.7	$0.11^{+0.08}_{-0.05}$	$8.89^{+4.10}_{-2.94}$
NGC 5236 (M 83)	2.6	0.36	1	4.7	$0.09^{+0.12}_{-0.05}$	$0.91^{+2.29}_{-0.84}$
NGC 5238 (Mkn 1479)	0.013	0.26	0	4.9	0	$0.00^{+1.83}_{-0.00}$
NGC 5408	0.09	0.11	1	4.85	0	$1.00^{+2.29}_{-0.83}$
NGC 5457 (M 101, Arp 26)	3.1	0.17	7	6.9	$0.40^{+0.34}_{-0.18}$	$6.60^{+3.77}_{-2.60}$

Table 1 - continued.

Table 1 - continued.

Galaxy	SFR ($M_{\odot} \text{ yr}^{-1}$)	Z (Z_{\odot})	$N_{\text{ULX, raw}}^{\text{a}}$	D (Mpc) ^b	Q^{c}	$N_{\text{ULX}}^{\text{d}}$
Circinus	1.5	0.1	4	4.2	$0.00^{+0.01}_{-0.00}$	$4.00^{+3.15}_{-1.91}$
NGC 6946 (Arp 29)	3.56	0.283	3	5.5	$0.08^{+0.11}_{-0.05}$	$2.92^{+2.91}_{-1.63}$
PGC 68618 (IC 5201)	1.7	0.260	1	11.1	$0.49^{+0.24}_{-0.16}$	$0.51^{+2.29}_{-0.51}$
NGC 7714/7715 (Arp 284, Mkn 538)	7.2	0.2	9	36.6	$0.84^{+0.14}_{-0.12}$	$8.16^{+4.11}_{-2.94}$
NGC 7742	1.27	0.245	2	22.2	$0.32^{+0.05}_{-0.05}$	$1.68^{+2.63}_{-1.29}$
Milky Way	0.25	0.306	0	—	0	$0.00^{+1.83}_{-0.00}$
IC 10	7.14×10^{-2}	0.22	0	0.70	0	$0.00^{+1.83}_{-0.00}$
Large Magellanic Cloud (LMC)	0.25	0.27	0	0.051	0	$0.00^{+1.83}_{-0.00}$
Small Magellanic Cloud (SMC)	0.15	0.129	0	0.064	0	$0.00^{+1.83}_{-0.00}$

Notes. The references for the values of SFR, Z and $N_{\text{ULX, raw}}$ reported in this Table are given in Appendix B. ^a $N_{\text{ULX, raw}}$ is the observed number of ULXs per galaxy, before the subtraction of contaminating sources. ^b D is the distance in Mpc (from the Liu & Bregman 2005 catalogue; if the galaxy is not in such catalogue, from the NASA Extragalactic Database). ^c Number of expected contaminating objects, estimated as described in Sections 2.2.1 and B4 (Appendix B). When Q is equal to zero (without uncertainties), either the contamination was already subtracted in $N_{\text{ULX, raw}}$ (i.e. in the paper with the original data) and $N_{\text{ULX, raw}} = N_{\text{ULX}}$, or $N_{\text{ULX, raw}} = 0$. ^d N_{ULX} is the observed number of ULXs per galaxy, after the subtraction of the estimated number of contaminating sources. The errors come from the combination of the Poissonian uncertainties upon $N_{\text{ULX, raw}}$ (according to the treatment in Gehrels 1986), and on Q (with uncertainties from the Hasinger et al. 1998 $\log(N) - \log(S)$ relation). ^e NGC 4501 is the only galaxy with $N_{\text{ULX}} > 0$ and with $Z > 0.47 Z_{\odot}$. For this galaxy $N_{\text{BH}} = 0$ in both P98 and B10 models (see Fig. 1 and Section 3.2), although $N_{\text{BH}} + 1\sigma > 0$.

ROSAT High Resolution Imager (HRI) with detection limits that would allow the detection of ULXs. Thus, the LB05 catalogue is less biased than LM05, as it includes galaxies with and without ULXs, and it is more homogeneous, as all the data reported come from the same instrument. On the other hand, even LB05 suffers from some observation bias (i.e., galaxies were originally chosen to be observed for a myriad different reasons), and the instrumental properties (especially sensitivity and resolution) of *ROSAT* are quite worse than those of *Chandra* and *XMM-Newton*, whose observations are included in LM05. Furthermore, some galaxies have been observed after 2004 and are not included in these catalogues, but there is no reason not to take them into account.

Given this situation, our sample is inevitably affected by various biases (e.g. galaxies without ULXs are likely under-represented) and it is not homogeneous. It is mainly based upon the LB05 catalogue, which includes 52 of the 64 galaxies listed in Table 1. The remaining 12 galaxies can be divided into 5 Local Group galaxies (NGC 598, the Milky Way, IC 10, and the two Magellanic Clouds), and 7 non-Local Group galaxies (the Cartwheel, the Antennae, the Mice, NGC 628, NGC 1058, NGC 5408, and Circinus). The 5 Local Group galaxies have low SFR (the average is $0.36 M_{\odot} \text{ yr}^{-1}$, compared to $2.06 M_{\odot} \text{ yr}^{-1}$ for the 52 LB05 galaxies) and a total of only one ULX (i.e. an average of 0.2 ULXs/galaxy, compared to 2.29 ULXs/galaxy in the 52 LB05 galaxies; here we are neglecting contamination); whereas the 7 non-local group galaxies have high SFR (average of $5.31 M_{\odot} \text{ yr}^{-1}$) and many ULXs (average of 6.86 ULXs/galaxy).

Each of the two non-LB05 sub-groups is clearly different from the sample of LB05 galaxies. However, we still include both of them in our sample, because they allow us to explore regimes that are not well represented by the 52 galaxies in LB05: the Local Group galaxies enlarge the number of galaxies with no ULXs, that are likely under-represented because of observation and publication bias; the non-Local Group

galaxies provide us with examples (such as the Cartwheel and the Antennae) of relatively rare objects with high SFR.

We note that, even if a galaxy is in the LB05 catalogue, we often use X-ray measurements coming from more recent papers where dedicated analysis have been published: Table 1 includes 27 galaxies for which the raw number of ULXs ($N_{\text{ULX, raw}}$, i.e. the observed number of ULXs per galaxy, before the subtraction of contaminating sources) is taken from LB05, 24 galaxies for which it is taken from LM05, and 13 galaxies for which $N_{\text{ULX, raw}}$ is taken from other papers.

2.2.1 Short description of Table 1

A full account of the origin of all the data reported in Table 1 will be given in Appendix B. Here we only provide a basic description of the most important quantities.

The SFRs come from either ultra-violet, $H\alpha$, far-infrared, radio measurements, or an average of these different measurements, depending on the data available for each galaxy. Galaxies whose SFR is highly uncertain (a factor of 10 or more), due, e.g., to the presence of an active galactic nucleus (AGN), are not considered in our sample (e.g. NGC 1068, NGC 3690). Concerning metallicity measurements, their existence is the most restrictive among our selection criteria, as metallicities are often unavailable. For most galaxies in the sample, we use measurements derived from line intensities in HII regions, translated into abundances with the empirical relation of Pilyugin (2001a; hereafter P01) or Pilyugin & Thuan (2005; hereafter PT05). If more than one HII region was measured within a galaxy, it is generally possible to derive the metallicity gradient; in such cases, we use the metallicity at the mean distance of ULXs from the centre of their host galaxy ($0.73 R_{25}$, where R_{25} is the radius of the 25th magnitude isophote; see Appendix B and Liu et al. 2006). When the spectra of HII regions are unavailable, we use X-ray measurements, although they are much less accurate.

The number of expected contaminating sources (Q)

Table 2. Values of N_{BH} and ϵ_{BH} for the galaxies listed in Table 1, assuming the models by P98 (first and second column) and by B10 (third and fourth column). We adopt a Kroupa IMF.

Galaxy	N_{BH} (P98)	$\epsilon_{\text{BH}}/10^{-4}$ (P98)	N_{BH} (B10)	$\epsilon_{\text{BH}}/10^{-4}$ (B10)
The Cartwheel	41900^{+21700}_{-21600}	$4.5^{+2.7}_{-2.6}$	70200^{+35200}_{-35400}	$2.7^{+1.6}_{-1.5}$
NGC 253	6070^{+3180}_{-3240}	$4.9^{+5.4}_{-3.8}$	11200^{+5700}_{-5900}	$2.7^{+2.9}_{-2.0}$
NGC 300	245^{+125}_{-130}	$0^{+74.7}_{-0}$	438^{+222}_{-224}	$0^{+41.8}_{-0}$
NGC 598	1280^{+710}_{-1280}	$7.8^{+18.4}_{-7.8}$	2510^{+1330}_{-1380}	$4.0^{+9.4}_{-4.0}$
NGC 628	2860^{+1570}_{-1550}	$6.7^{+9.9}_{-5.9}$	5440^{+2880}_{-2850}	$3.5^{+5.2}_{-3.0}$
NGC 1058	377^{+198}_{-203}	$24.1^{+62.1}_{-24.1}$	709^{+374}_{-371}	$12.8^{+33.0}_{-12.8}$
NGC 1073	1290^{+730}_{-1290}	$15.5^{+22.2}_{-15.5}$	2620^{+1390}_{-1450}	$7.6^{+10.8}_{-6.3}$
NGC 1291	2730^{+1370}_{-1380}	$10.6^{+11.9}_{-8.1}$	3690^{+1860}_{-1850}	$7.9^{+8.8}_{-6.0}$
NGC 1313	3460^{+1760}_{-1750}	$5.8^{+8.1}_{-4.7}$	5100^{+2580}_{-2560}	$3.9^{+5.5}_{-3.2}$
NGC 1365	12600^{+6400}_{-6700}	$6.5^{+4.7}_{-4.2}$	20900^{+11000}_{-10600}	$5.8^{+3.8}_{-3.4}$
IC 342	841^{+451}_{-435}	$23.5^{+33.7}_{-19.7}$	1500^{+760}_{-770}	$13.2^{+18.7}_{-11.0}$
NGC 1566	3560^{+1990}_{-3560}	$7.0^{+10.3}_{-7.0}$	6780^{+3730}_{-3570}	$3.7^{+5.4}_{-3.7}$
NGC 1705	153^{+81}_{-95}	$0^{+19.6}_{-0}$	274^{+139}_{-142}	$0^{+66.8}_{-0}$
NGC 2366	185^{+94}_{-95}	$0^{+98.9}_{-0}$	272^{+138}_{-136}	$0^{+67.3}_{-0}$
NGC 2403	637^{+333}_{-339}	$15.7^{+36.9}_{-15.5}$	1160^{+600}_{-600}	$8.6^{+20.2}_{-8.4}$
NGC 2442	0^{+5270}_{-0}	> 1.3	5930^{+4370}_{-5930}	$1.1^{+4.9}_{-1.1}$
Holmberg II	247^{+125}_{-125}	$40.4^{+95.00}_{-39.4}$	364^{+184}_{-182}	$27.5^{+64.4}_{-26.6}$
NGC 2903	2440^{+1340}_{-1370}	$7.8^{+11.6}_{-7.0}$	4640^{+2450}_{-2430}	$4.1^{+6.1}_{-3.6}$
NGC 3031	4300^{+2360}_{-2320}	$4.6^{+6.6}_{-3.9}$	8180^{+4330}_{-4280}	$2.4^{+3.5}_{-2.0}$
NGC 3049	0^{+0}_{-0}	—	0^{+0}_{-0}	—
PGC 30819	110^{+56}_{-58}	$0^{+166.4}_{-0}$	187^{+95}_{-96}	$0^{+97.9}_{-0}$
NGC 3310	3510^{+1890}_{-1870}	$8.1^{+9.4}_{-6.4}$	6380^{+3280}_{-3320}	$4.4^{+5.1}_{-3.5}$
NGC 3395/3396	7490^{+4040}_{-3990}	$9.3^{+7.1}_{-6.1}$	13600^{+7000}_{-7000}	$5.1^{+3.8}_{-3.2}$
PGC 35286	48^{+24}_{-24}	$0^{+381.2}_{-0}$	68^{+34}_{-34}	$0^{+269.1}_{-0}$
PGC 35684	25^{+13}_{-13}	$0^{+732.0}_{-0}$	38^{+19}_{-19}	$0^{+481.6}_{-0}$
NGC 3738	63^{+33}_{-33}	$0^{+290.5}_{-0}$	114^{+58}_{-58}	$0^{+160.5}_{-0}$
NGC 3972	310^{+174}_{-310}	$0^{+59.03}_{-0}$	628^{+334}_{-348}	$0^{+29.1}_{-0}$
Antennae	22200^{+11100}_{-11200}	$6.7^{+4.0}_{-3.8}$	30000^{+15000}_{-15000}	$5.0^{+3.0}_{-2.8}$
NGC 4144	84^{+44}_{-45}	$0^{+217.9}_{-0}$	151^{+76}_{-77}	$0^{+121.2}_{-0}$
NGC 4214	213^{+115}_{-110}	$0^{+85.9}_{-0}$	404^{+204}_{-210}	$0^{+45.3}_{-0}$
NGC 4236	191^{+100}_{-102}	$0^{+95.8}_{-0}$	348^{+176}_{-181}	$0^{+52.6}_{-0}$
NGC 4248	25^{+14}_{-14}	$0^{+732.0}_{-0}$	48^{+25}_{-25}	$0^{+381.2}_{-0}$
NGC 4254	5480^{+2880}_{-2950}	$2.9^{+5.9}_{-2.9}$	10700^{+5500}_{-5600}	$1.5^{+3.0}_{-1.5}$
NGC 4258	2900^{+1610}_{-2900}	$8.3^{+11.2}_{-8.3}$	5690^{+3010}_{-3130}	$4.3^{+5.7}_{-3.9}$
NGC 4303	9700^{+5050}_{-5150}	$4.2^{+4.5}_{-3.6}$	16800^{+8900}_{-8500}	$2.4^{+2.6}_{-2.0}$
NGC 4321	6240^{+3420}_{-3370}	$8.2^{+7.8}_{-6.4}$	11900^{+6300}_{-6200}	$4.3^{+4.1}_{-3.3}$
NGC 4395	197^{+107}_{-105}	$48.7^{+119.2}_{-48.7}$	359^{+185}_{-187}	$26.7^{+65.3}_{-27.5}$
NGC 4449	408^{+214}_{-219}	$0^{+44.8}_{-0}$	759^{+400}_{-396}	$0^{+24.1}_{-0}$
NGC 4485/4490	6870^{+3600}_{-3670}	$7.1^{+6.2}_{-5.0}$	12600^{+6500}_{-6600}	$3.9^{+3.3}_{-2.7}$
NGC 4501	0^{+3180}_{-0}	> 4.1	0^{+6710}_{-0}	> 1.9
NGC 4559	2370^{+1230}_{-1260}	$8.4^{+11.9}_{-7.0}$	4240^{+2150}_{-2200}	$4.7^{+6.6}_{-3.9}$
NGC 4631	4450^{+2400}_{-2370}	$4.1^{+6.3}_{-3.7}$	8090^{+4160}_{-4220}	$2.3^{+3.5}_{-2.0}$
NGC 4651	2080^{+1130}_{-1080}	$4.0^{+11.2}_{-4.0}$	3970^{+2010}_{-2070}	$2.1^{+5.9}_{-2.1}$
NGC 4656	2550^{+1290}_{-1290}	$3.7^{+9.2}_{-3.7}$	3720^{+1870}_{-1870}	$2.6^{+6.3}_{-2.6}$
The Mice	6980^{+3870}_{-6980}	$8.6^{+7.0}_{-8.6}$	13700^{+7500}_{-7200}	$4.4^{+3.6}_{-2.9}$
NGC 4736	1930^{+980}_{-1020}	$4.4^{+12.1}_{-4.4}$	3310^{+1710}_{-1700}	$2.6^{+7.0}_{-2.6}$
NGC 4861	1300^{+670}_{-670}	$14.6^{+21.6}_{-12.7}$	2080^{+1040}_{-1040}	$9.1^{+13.4}_{-7.8}$
PGC 45561	0^{+377}_{-0}	$0^{+48.5}_{-0}$	531^{+295}_{-531}	$0^{+34.5}_{-0}$
NGC 5033	4050^{+2050}_{-2030}	$3.4^{+6.9}_{-3.4}$	5920^{+2970}_{-2970}	$2.3^{+4.7}_{-2.3}$
NGC 5055	2040^{+1130}_{-2040}	$8.9^{+13.8}_{-8.9}$	3990^{+2110}_{-2090}	$4.6^{+7.0}_{-4.2}$
NGC 5194/5195	0^{+17300}_{-0}	> 5.2	23300^{+13600}_{-23300}	$3.8^{+2.8}_{-3.8}$
NGC 5236	0^{+3580}_{-0}	> 2.5	4990^{+2660}_{-3620}	$1.8^{+4.7}_{-1.8}$
NGC 5238	18^{+10}_{-10}	$0^{+1017.0}_{-0}$	35^{+18}_{-18}	$0^{+522.9}_{-0}$
NGC 5408	223^{+113}_{-113}	$44.8^{+105.2}_{-43.6}$	328^{+166}_{-164}	$30.5^{+71.5}_{-29.6}$
NGC 5457	5890^{+2990}_{-3110}	$11.2^{+8.6}_{-7.4}$	9610^{+4870}_{-4860}	$6.9^{+5.2}_{-4.4}$

Table 2 - continued.

Table 2 - continued.

Galaxy	N_{BH} (P98)	$\epsilon_{\text{BH}}/10^{-4}$ (P98)	N_{BH} (B10)	$\epsilon_{\text{BH}}/10^{-4}$ (B10)
Circinus	3710^{+1880}_{-1880}	$10.8^{+10.1}_{-7.5}$	5460^{+2760}_{-2740}	$7.3^{+6.8}_{-5.1}$
NGC 6946	4630^{+2540}_{-2500}	$6.3^{+7.2}_{-4.9}$	8820^{+4660}_{-4610}	$3.3^{+3.7}_{-2.5}$
PGC 68618	2330^{+1220}_{-1250}	$2.2^{+10.1}_{-2.2}$	4560^{+2350}_{-2430}	$1.1^{+5.2}_{-1.1}$
NGC 7714/7715	12600^{+6400}_{-6700}	$9.7^{+6.2}_{-5.9}$	22500^{+11400}_{-11700}	$3.6^{+2.6}_{-2.3}$
NGC 7742	1830^{+1000}_{-980}	$9.2^{+15.3}_{-9.1}$	3400^{+1800}_{-1780}	$4.9^{+8.2}_{-4.9}$
Milky Way	291^{+161}_{-291}	$0^{+62.9}_{-0}$	570^{+302}_{-299}	$0^{+32.1}_{-0}$
IC 10	114^{+61}_{-178}	$0^{+160.5}_{-0}$	207^{+107}_{-108}	$0^{+88.4}_{-0}$
LMC	325^{+176}_{-176}	$0^{+56.3}_{-0}$	618^{+327}_{-323}	$0^{+29.6}_{-0}$
SMC	314^{+167}_{-159}	$0^{+58.3}_{-0}$	526^{+264}_{-264}	$0^{+34.8}_{-0}$

with apparent luminosities $\geq 10^{39} \text{ erg s}^{-1}$ was calculated on the basis of the Hasinger et al. (1998) $\log(N)$ - $\log(S)$ relation, using the distance D and other quantities listed in Appendix B (e.g. R_{25} , which was taken from the RC3 catalogue of de Vaucouleurs et al. 1991).

Finally, the number N_{ULX} of ULXs in a galaxy after the subtraction of contaminating sources is simply $N_{\text{ULX}} = N_{\text{ULX,raw}} - Q$.

2.3 Uncertainties and fitting procedures

In the following, we consider various sources of error for the different considered quantities (SFR, Z , N_{ULX}).

For the SFR, we assume that the relative uncertainty of each value is ± 0.5 . This number comes from the analysis of the distribution of the measurements reported in Grimm et al. (2003): the SFR measurements reported in columns 7, 8, 9, and 10 of their table 3 were normalized to the ‘adopted SFR’ reported in column 11 of the same table; the distribution of the resulting values is bell-shaped and centred around 1; furthermore, about 68 per cent of them lies between 0.5 and 1.5.

We assume that all the metallicity measurements are uncertain by 0.1 dex, which is the typical error associated with metallicity measurements in HII regions (see e.g. P01; Kennicutt et al. 2003; PT05)⁴.

We note that the uncertainty on the SFR affects the error on N_{BH} in a linear way; instead, because of the complicated dependence of N_{BH} upon Z (N_{BH} changes very rapidly with Z for $Z \sim 0.3 - 0.4 Z_{\odot}$, whereas it is almost independent of Z for $Z \gtrsim 0.5 Z_{\odot}$ or $Z \lesssim 0.2 Z_{\odot}$), the uncertainty in Z can result in both very small and very large errors on N_{BH} (this explains the upper limits that can be seen in the left-hand panel of Fig. 2).

In the case of $N_{\text{ULX,raw}}$ we adopt Poisson uncertainties, as they are affected by small-number fluctuations (Grimm et al. 2003). These are estimated through the treatment described in Gehrels (1986). Instead, in the case of Q we simply assume uncertainties coming from errors upon the $\log(N) - \log(S)$ of Hasinger et al. (1998).

Finally, the uncertainties on N_{ULX} derive from the combination of the two above uncertainties.

The analysis presented in the following sections is based upon correlation coefficients and power-law fits. Fits were performed by minimizing χ^2 . However, since, in most cases, the quantities on both axes have uncertainties of similar (relative) magnitude, we keep both errors into account through the simple procedures summarized in D’Agostini (2005).

We note that this fact, along with the sizable error bars of the variables, tends to produce values of χ^2 that are significantly lower than the number of degrees of freedom (hereafter, dof). However, in the low-number regime (that we are considering here) the difference between Poissonian and Gaussian statistics become significant and hence, whenever possible, we checked our results adopting additional fits based on Cash statistics (Cash 1979). In such cases, we further note that i) fits with Cash statistics do *not* consider the errors on the quantity on the x -axis, and ii) in the cases where the variable on the y -axis is N_{ULX} , we actually performed a fit to $N_{\text{ULX,raw}}$ with the sum of the contamination Q to the results of the fitting formula, as required by the Cash formalism. The results of the fits based on Cash statistics are in reasonably good agreement with those of the fits based on χ^2 . The main difference is that the Cash statistics appears to better constrain the parameters and give smaller errors, although this follows in part from neglecting uncertainties on the x -axis. In any case, this result reinforces the validity of our analysis.

3 RESULTS

3.1 Expected number of massive BHs versus observed number of ULXs

Table 2 shows the values of N_{BH} and ϵ_{BH} (the role of ϵ_{BH} is discussed in Appendix C) that we derive for the galaxies listed in Table 1, using the models by P98 and by B10. In paper I, we showed that, according to theoretical models (Patruno et al. 2005; Blecha et al. 2006), ϵ_{BH} should be of the order of 10^{-4} for the Kroupa IMF, which is consistent with most values in Table 2 (especially for the models adopting B10 and for galaxies with a large number of ULXs). In Fig. 2, we show the observed number of ULXs per galaxy, N_{ULX} , as a function of the expected number of massive BHs per galaxy, N_{BH} .

From Fig. 2 it is immediately evident that there is a correlation between N_{BH} and N_{ULX} , when we adopt the models from both P98 and B10. Such correlation can be expressed as:

⁴ The actual error might be larger for several reasons, such as uncertainties in the metallicity calibrations, or metallicity fluctuations within a single galaxy (even at a given radius).

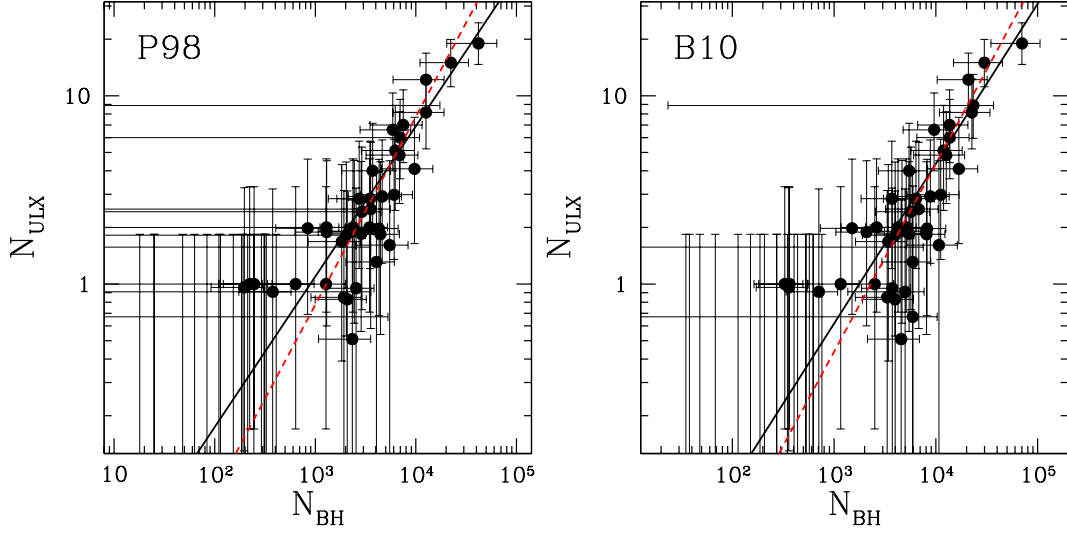


Figure 2. Left-hand panel: Number of observed ULXs per galaxy N_{ULX} versus the number of expected massive BHs per galaxy N_{BH} , derived using the models from P98. The adopted IMF is a Kroupa IMF (see Appendix A for a comparison with the Salpeter IMF). The filled circles are the galaxies listed in Table 1. The solid line is the power-law fit for the entire sample. The dashed line (red on the web) is the power-law fit obtained assuming that the index of the power law is $\beta = 1$. The error bars on both the x - and the y - axis are $1 - \sigma$ errors. The error bars on N_{BH} account for the uncertainty on the SFR and on the metallicity (see Section 2.3 for details). Right-hand panel: the same as the left-hand panel, but the number of expected massive BHs per galaxy, N_{BH} , has been derived using the models from B10.

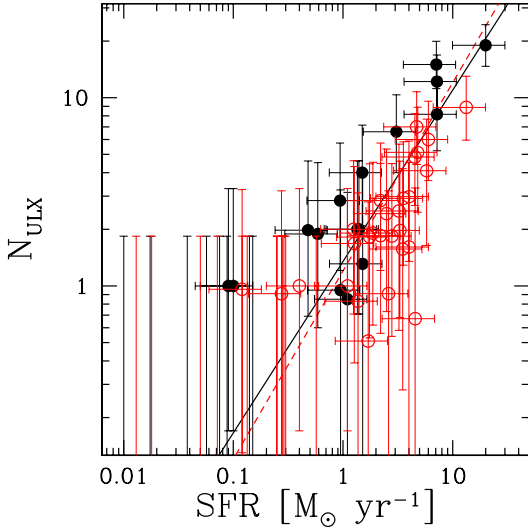


Figure 3. N_{ULX} versus the SFR. Filled black circles: galaxies with metallicity $\leq 0.2 Z_{\odot}$; open circles (red on the web): galaxies with metallicity $> 0.2 Z_{\odot}$. Solid line: power-law fit for the entire sample; dashed line (red on the web): power-law fit obtained assuming that the index of the power law is $\delta_1 = 1$. The error bars on both the x - and the y - axis are $1 - \sigma$ errors (see Section 2.3 for details).

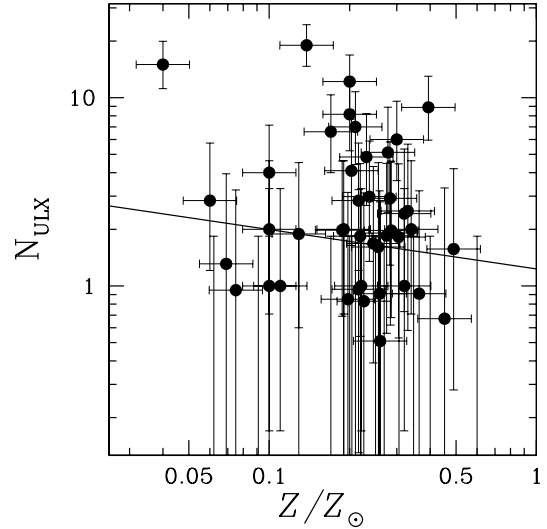


Figure 4. N_{ULX} versus Z . Filled black circles: entire sample; solid line: power-law fit. The error bars on both the x - and the y - axis are $1 - \sigma$ errors (see Section 2.3 for details).

p_r to obtain⁵ a correlation coefficient with an absolute value larger than $|r|$ if the two variables were uncorrelated.

The correlation coefficient r is very high, and the probability of finding a value larger than $|r|$, if the two variables

$$N_{\text{ULX}} = 10^{\gamma} N_{\text{BH}}^{\beta}, \quad (5)$$

where $\beta = 0.80^{+0.16}_{-0.12}$ ($\beta = 0.85^{+0.19}_{-0.13}$) and $\gamma = -2.36^{+0.45}_{-0.62}$ ($\gamma = -2.76^{+0.53}_{-0.76}$), when adopting the models from P98 (B10). Table 3 reports the fits, the results of the χ^2 analysis, the Pearson correlation coefficients (r), and the probability

⁵ Such probability is based on the assumption that the two variables whose correlation is being tested are normally distributed. This is likely not the case for our data; however, the value of p_r can still be retained as an indicator of the strength (or weakness) of a correlation.

were uncorrelated and normally distributed, is almost zero. The values of the χ^2 associated with the best fits of the $N_{\text{BH}} - N_{\text{ULX}}$ relation are $\chi^2 \lesssim 12$, with 62 degrees of freedom (dof). The χ^2 is almost as low when an index $\beta = 1.00$ is assumed. According to the F-test (see paragraph 10.2 in Bevington 1969), the above fit with two parameters (see lines 1 and 3 of Table 3) is better than a fit with fixed index $\beta = 1$ (see lines 2 and 4 of Table 3) only at 91 and 80 per cent confidence level in the case of P98 and B10, respectively. This implies that, especially for B10, the fit with two parameters is not a significant improvement. This suggests that the $N_{\text{BH}} - N_{\text{ULX}}$ correlation is a linear relation, although deviations from a linear behaviour are possible⁶.

Furthermore, the slopes are very similar for the two considered models of stellar evolution. The main difference between them is the normalization, as the values of N_{BH} obtained assuming P98 are generally a factor of 1.5–2 lower than the values obtained using B10.

Finally, from Tables 2–3 and from Fig. 2, it appears that the galaxies in our sample that do not host any ULXs have very low values of N_{BH} : according to our model, they are consistent with having one or zero ULXs.

In conclusion, Fig. 2 and Tables 2 and 3 indicate that our model predicts a number of massive BHs that correlates with the number of ULXs per galaxy, independently of the adopted stellar evolution scenario. Such correlation supports the hypothesis that (all or a large fraction of) the ULXs are connected with massive ($m_{\text{BH}} \geq 25 M_{\odot}$) BHs.

3.2 Dependence on the SFR and on the metallicity

Our model is based on two key parameters: SFR and metallicity. In this Subsection we discuss their role in more detail.

3.2.1 Star formation rate

As mentioned in the Introduction, the existence of a correlation between SFR and number of bright X-ray sources per galaxy is well established (Grimm et al. 2003; Ranalli et al. 2003; Gilfanov et al. 2004a,b,c). From Fig. 3, it is evident that our sample of galaxies follows the same correlation, which can be fit as:

$$N_{\text{ULX}} = 10^{\zeta} \left(\frac{\text{SFR}}{M_{\odot} \text{ yr}^{-1}} \right)^{\delta}, \quad (6)$$

where $\delta = 0.91^{+0.25}_{-0.15}$ and $\zeta = 0.13^{+0.10}_{-0.14}$ (with $\chi^2 \sim 18$ for 62 dof, see Table 3), if we consider all the galaxies in the sample. We note that the index of the correlation (δ) is smaller than 1, but consistent with 1. Furthermore, the value of the χ^2 is very low ($\chi^2 \sim 18$ with 63 dof), even when we assume $\delta = 1.00$. According to the F-test, the above fit with two parameters (see line 5 of Table 3) is better than a fit with fixed index $\delta = 1$ (see line 6 of Table 3) only at 48 per cent

confidence level. This means that the fit with two parameters is not an improvement.

If we impose $\delta = 1.00$, we obtain $N_{\text{ULX}} \simeq 1.20^{+0.18}_{-0.15}$ SFR. Likewise, Grimm et al. (2003) find an almost linear relation between the SFR and the number of X-ray sources with $L_X \geq 2 \times 10^{38} \text{ erg s}^{-1}$. Our best-fitting slope in the linear relation ($1.20^{+0.18}_{-0.15}$) is a factor of 2.4 ± 0.4 lower than the value (2.9 ± 0.23) reported by Grimm et al. (2003); given the different luminosity ranges ($L_X \geq 2 \times 10^{38} \text{ erg s}^{-1}$ and $L_X \geq 10^{39} \text{ erg s}^{-1}$ in Grimm et al. 2003 and in this Paper, respectively), this is expected. In fact, equation (7) of Grimm et al. (2003) predicts a factor 3.0 ± 0.5 difference between the normalizations of the correlations in the two luminosity ranges, consistent with our result (the uncertainty is due to the error on the slope of the luminosity function given in Equation 6 of Grimm et al. 2003).

We remind also that, in our model, we imposed that N_{BH} scales linearly with the SFR (see equation 3), in agreement with the observational behaviour of N_{ULX} . Lines 13–14 of Table 3 indicate that our fitting procedure infers a slope which is consistent with the theoretical value within a ± 0.06 uncertainty. The normalization for the model by P98 is a factor of $\sim 1.5 - 2$ lower than that of the model by B10.

3.2.2 Metallicity

In Paper I we proposed that there may be an anticorrelation between the observed number of ULXs (N_{ULX}) and the metallicity (Z), but our sample was too small to confirm such anticorrelation. Our current sample is more than three times larger than the one in Paper I.

In the current paper, a first argument in favour of the role played by the metallicity comes from Fig. 3 (i.e. N_{ULX} versus SFR): it is evident that the galaxies with $Z > 0.2 Z_{\odot}$ (open circles) lie mostly below the global fit, whereas the galaxies with $Z \leq 0.2 Z_{\odot}$ (filled circles) lie preferentially above the global fit. This means that a metal-poor ($Z \leq 0.2 Z_{\odot}$) galaxy tends to have more ULXs with respect to a relatively metal-rich ($Z > 0.2 Z_{\odot}$) galaxy with the same SFR. In quantitative terms, Table 3 shows that, if we split our sample according to metallicity and fit the SFR– N_{ULX} relation, we obtain similar slopes, but quite different values of the normalization for the high- Z sample ($\zeta_1 = 0.05^{+0.13}_{-0.20}$) and for the low- Z sample ($\zeta_1 = 0.39^{+0.09}_{-0.13}$). The difference ($0.34^{+0.22}_{-0.18}$; or 0.32 ± 0.14 if the slope is fixed to $\delta = 1.00$) is not consistent with 0 at a significance level slightly below 2σ , while it is roughly consistent with the ratio of the expected numbers of massive BHs below and above $Z \sim 0.2 Z_{\odot}$ (see Fig. 1). This might be a further indication that the SFR is not the only ingredient of the correlation between N_{BH} and N_{ULX} and that the second ingredient might actually be the metallicity, as proposed in our model.

However, we cannot conclude from Fig. 4 and from Table 3 that such anticorrelation exists. There is a very weak trend that can be expressed as

$$N_{\text{ULX}} = 10^{\theta} (Z/Z_{\odot})^{\eta}, \quad (7)$$

where $\eta = -0.21 \pm 0.27$ and $\theta = 0.09 \pm 0.20$. Such trend is not statistically significant, as $\chi^2 = 86$ with 62 dof and the correlation coefficient is $r \lesssim -0.2$, with $p_r = 0.2$ (Table 3).

Similarly to equation (7), there is no significant anticorrelation, in our model, between N_{BH} and Z (lines 15–16 of

⁶ The scaling between N_{BH} and N_{ULX} might be non-linear because N_{ULX} may depend also on properties that do not affect N_{BH} , such as the probability of finding sufficiently massive companion stars. Thus, a better understanding of the properties of HMXBs that can power ULXs is needed, in order to refine our model.

Table 3. Parameters of the power-law fits and χ^2 .

x -axis	y -axis	Model	Sample ^a	Index ^{b,c}	Normalization ^c	χ^2/dof ^d	r (pr) ^e
N_{BH}	N_{ULX}	P98	all	$0.80^{+0.16}_{-0.12} (0.86 \pm 0.07)$	$-2.36^{+0.45}_{-0.62} (-2.64 \pm 0.28)$	8.7/62	$0.90 (2 \times 10^{-23})$
N_{BH}	N_{ULX}	P98	all	1.00(1.00)	$-3.11 \pm 0.07 (-3.17 \pm 0.04)$	10.0/63	$0.90 (2 \times 10^{-23})$
N_{BH}	N_{ULX}	B10	all	$0.85^{+0.19}_{-0.13} (0.90 \pm 0.07)$	$-2.76^{+0.53}_{-0.76} (-3.00 \pm 0.30)$	11.1/62	$0.93 (1 \times 10^{-27})$
N_{BH}	N_{ULX}	B10	all	1.00(1.00)	$-3.36 \pm 0.07 (-3.41 \pm 0.04)$	11.8/63	$0.93 (1 \times 10^{-27})$
SFR	N_{ULX}	–	all	$0.91^{+0.25}_{-0.15} (0.90 \pm 0.08)$	$0.13^{+0.10}_{-0.14} (0.09 \pm 0.06)$	17.7/62	$0.88 (4 \times 10^{-22})$
SFR	N_{ULX}	–	all	1.00(1.00)	$0.08 \pm 0.06 (0.02 \pm 0.04)$	17.8/63	$0.88 (4 \times 10^{-22})$
SFR	N_{ULX}	–	lowZ	$0.75^{+0.20}_{-0.13} (0.80 \pm 0.08)$	$0.39^{+0.09}_{-0.13} (0.32 \pm 0.07)$	4.4/22	$0.93 (8 \times 10^{-11})$
SFR	N_{ULX}	–	highZ	$0.83^{+0.37}_{-0.22} (0.94 \pm 0.15)$	$0.05^{+0.13}_{-0.20} (-0.06 \pm 0.10)$	6.4/38	$0.88 (6 \times 10^{-14})$
Z/Z_{\odot}	N_{ULX}	–	all	$-0.21 \pm 0.27 (-0.55 \pm 0.15)$	$0.09 \pm 0.20 (-0.04 \pm 0.12)$	86.0/62	$-0.16 (2 \times 10^{-1})$
Z/Z_{\odot}	N_{ULX}	–	all	0.00(0.00)	$0.23 \pm 0.05 (0.36 \pm 0.04)$	86.6/63	$-0.16 (2 \times 10^{-1})$
Z/Z_{\odot}	$N_{\text{ULX}}/\text{SFR}$	–	all	-0.55 ± 0.23	-0.37 ± 0.18	10.4/62	$-0.30 (2 \times 10^{-2})$
Z/Z_{\odot}	$N_{\text{ULX}}/\text{SFR}$	–	all	0.00	-0.03 ± 0.07	14.7/63	$-0.30 (2 \times 10^{-2})$
SFR	N_{BH}^{f}	P98	all	0.96 ± 0.06	3.19 ± 0.04	13.8/62	$0.82 (7 \times 10^{-17})$
SFR	N_{BH}^{f}	B10	all	0.97 ± 0.05	3.44 ± 0.04	6.3/62	$0.95 (6 \times 10^{-33})$
Z/Z_{\odot}	N_{BH}^{f}	P98	all	-0.19 ± 0.29	$1.41^{+0.23}_{-0.26}$	153.9/62	$-0.23 (7 \times 10^{-2})$
Z/Z_{\odot}	N_{BH}^{f}	B10	all	$0.05^{+0.30}_{-0.27}$	1.85 ± 0.24	183.2/62	$-0.11 (4 \times 10^{-1})$
Z/Z_{\odot}	$N_{\text{BH}}/\text{SFR}^{\text{f}}$	P98	all	-0.60 ± 0.07	2.79 ± 0.05	9.4/62	$-0.96 (2 \times 10^{-37})$
Z/Z_{\odot}	$N_{\text{BH}}/\text{SFR}^{\text{f}}$	B10	all	$-0.34^{+0.02}_{-0.05}$	3.22 ± 0.04	17.0/62	$-0.98 (3 \times 10^{-48})$

The SFRs used by the fitting procedure are in units of $M_{\odot} \text{ yr}^{-1}$. ^a The sample adopted for the fits is referred to as ‘all’ when all the galaxies in Table 1 are considered, and as lowZ (highZ) when only the galaxies with $Z \leq 0.2 Z_{\odot}$ ($Z > 0.2 Z_{\odot}$) are considered. ^b When the index is equal to 1.00 or to 0.00, without error, it means that it has been fixed to such value. ^c Values in parenthesis are the fitting parameters obtained with Cash statistics (where applicable), rather than χ^2 ; such results do not take into account the uncertainty on the quantity on the x -axis. ^d χ^2/dof is the χ^2 divided by the degrees of freedom (dof). ^e r is the Pearson correlation coefficient, and pr is the probability of finding a value larger than $|r|$, if the two variables were uncorrelated and normally distributed. ^f The fits listed in rows 13–18 refer entirely to the theoretical model. We report them only for a comparison between the statistical fluctuations of the theoretical calculations and those of the observational data.

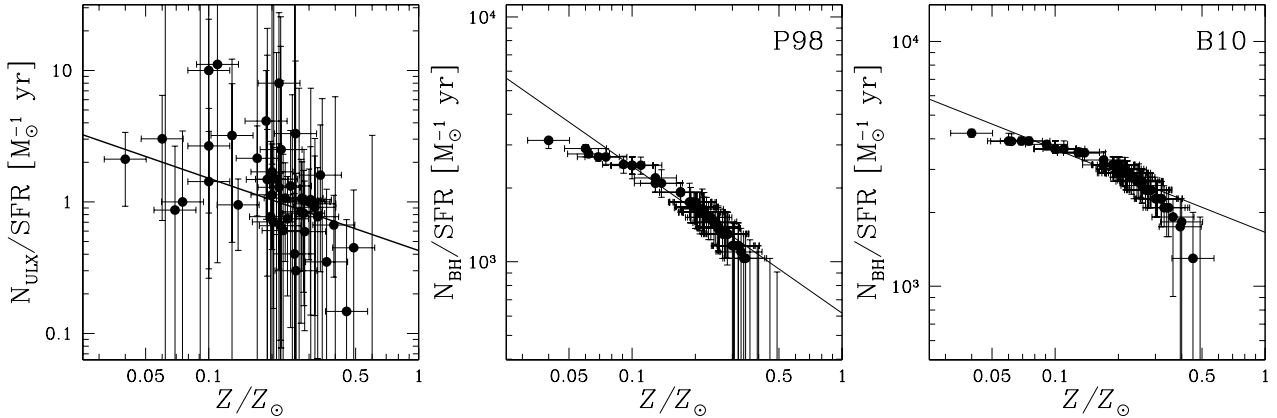


Figure 5. From left to right: $N_{\text{ULX}}/\text{SFR}$ versus Z , N_{BH}/SFR versus Z for P98, N_{BH}/SFR versus Z for B10. Filled black circles: entire sample. Solid lines: power-law fit. The error bars on both the x - and the y -axis are $1 - \sigma$ errors. Central and right-hand panel: the error bars on N_{BH}/SFR account for the uncertainty on the metallicity (see Section 2.3 for details).

Table 3). In particular, the values of the χ^2 for the best fits are 154 and 183 for P98 and B10, respectively, with 62 dof (see lines 15 and 16 of Table 3). The correlation coefficients are low: $r = -0.2$ and $r = -0.1$ for P98 and B10, respectively. This happens because, in our model, the dependence of N_{BH}

on the SFR dominates with respect to the dependence of N_{BH} on the metallicity.

To better highlight the possible effects of metallicity, we plot the number of ULXs per galaxy N_{ULX} normalized to the SFR versus the metallicity (left-hand panel of Fig. 5).

The fit of the left-hand panel in Fig. 5 gives the following results.

$$\left(N_{\text{ULX}} \frac{M_{\odot} \text{ yr}^{-1}}{\text{SFR}} \right) = 10^{\kappa_1} (Z/Z_{\odot})^{\iota_1}, \quad (8)$$

where $\iota_1 = -0.55 \pm 0.23$ and $\kappa_1 = -0.37 \pm 0.18$, with $\chi^2 \sim 10$ for 62 dof (and $r = -0.3$). Thus, there is marginal evidence of an anticorrelation between Z and $N_{\text{ULX}}/\text{SFR}$. According to the F-test, the above fit with two parameters (see line 11 of Table 3) is significantly better (at a 96 per cent significance level) than a fit with fixed index $\iota_1 = 0$ (i.e. the case of no correlation) and with only one free parameter ($\kappa_1 = -0.03 \pm 0.07$, line 12 of Table 3). This result supports the hypothesis of an anti-correlation between $N_{\text{ULX}}/\text{SFR}$ and Z .

As in the case of the comparison with N_{ULX} , the role of metallicity in our model can be better appreciated if we remove the contribution from the SFR. In fact, the plot of N_{BH}/SFR versus Z (central and right-hand panels of Fig. 5) shows quite clearly the effect of metallicity in equation (1). We know from equation (1) that the relation between N_{BH}/SFR and Z is not a power-law. However, in order to compare it with equation (8), we can approximate it as:

$$\left(N_{\text{BH}} \frac{M_{\odot} \text{ yr}^{-1}}{\text{SFR}} \right) = 10^{\kappa_2} (Z/Z_{\odot})^{\iota_2}, \quad (9)$$

where $\iota_2 = -0.60 \pm 0.07$ ($-0.34^{+0.02}_{-0.05}$) and $\kappa_2 = 2.79 \pm 0.05$ (3.22 ± 0.04) for P98 (B10). The statistical significance of such correlations is given in lines 17–18 of Table 3. ι_1 is consistent with ι_2 in the case of P98 and marginally consistent with ι_2 in the case of B10. Thus, we can conclude that the anticorrelation in the central and right-hand panels of Fig. 5 is consistent with that in the left-hand panel of the same Figure, although the error bars are quite large.

The fact that the anticorrelation between Z and N_{ULX} only emerges after removing the effect of the SFR (i.e. considering $N_{\text{ULX}}/\text{SFR}$ versus Z) clearly shows that the SFR (and not the metallicity) is the dominant factor in determining the number of ULXs in a given galaxy⁷. However, the metallicity plays a crucial role in enabling the formation of ULXs, as massive BHs can be produced only in star-forming regions where Z is sufficiently low.

We emphasize that, in our model, the effect of the metallicity on the formation of massive BHs is mainly a threshold effect: in the models by B10 (see their fig. 1 and their equation 11) massive ($m_{\text{BH}} \geq 25 M_{\odot}$) BHs form only for $Z \leq 0.47 Z_{\odot}$. If the metallicity Z is below this threshold, there is quite a small spread in m_{prog} (defined in equation 1) and thus in N_{BH} for various metallicities (at fixed SFR): adopting the model by B10, m_{prog} ranges from $68 M_{\odot}$ for $Z = 0.04 Z_{\odot}$ (the Antennae) to $96 M_{\odot}$ for $Z = 0.45 Z_{\odot}$ (NGC 2442). Furthermore, as N_{BH} scales linearly with the SFR, the effect of metallicity on N_{BH} is small with respect to the effect of the SFR, for $Z < 0.47 Z_{\odot}$.

Instead, if $Z > 0.47 Z_{\odot}$, massive BHs cannot form from the direct collapse of massive stars. This might be a problem for our model, as ULXs exist also in a few galaxies with $Z > 0.47 Z_{\odot}$: NGC 4501 (see Table 1) is the only galaxy, for which we found SFR, Z and X-ray data, that has

$N_{\text{ULX, raw}} > 0$ and $Z > 0.47 Z_{\odot}$. In such a case, the contamination from foreground/background sources ($Q = 0.43^{+0.11}_{-0.09}$) is not completely negligible; nonetheless it is insufficient to explain the 2 observed ULXs. However, there are several reasons for which this might happen.

First, as the metallicity is uncertain by ~ 0.1 dex, values of Z below $0.47 Z_{\odot}$ are well within 1σ error ranges for NGC 4501 ($1-\sigma$ lower limit on Z is $0.39 Z_{\odot}$ for NGC 4501). Thus, the upper limits of N_{BH} for NGC 4501 are larger than zero.

Second, in the case of large spiral galaxies (such as NGC 4501) our choice of taking the metallicity at $R = 0.73 R_{25}$, although justified, is rather simplistic: in NGC 4501 the metallicity gradient is such that Z goes below $0.4 Z_{\odot}$ at $R \leq R_{25}$, so that there exists a small region where massive BHs might form, even in the P98 model. Thus, uncertainties in the metallicity determination and spatial abundance fluctuations might further help in this respect.

Third, in this Paper we considered only BHs with $m_{\text{BH}} \geq 25 M_{\odot}$ as engines of the ULXs, but slightly less massive BHs might still power many low-luminosity ULXs, provided that there is a certain level of beaming or super-Eddington accretion (e.g. King 2008): for example, if the metallicity is $Z \lesssim 0.57 Z_{\odot}$ BHs with $m_{\text{BH}} \sim 20 M_{\odot}$ can still form (B10). It is worth mentioning that NGC 4501 hosts relatively faint ULXs, that can be explained without invoking massive BHs, nor strong beaming/super-Eddington accretion.

Finally, the metallicity needed in our model is that of the molecular clouds before the pollution from the first supernovae associated with the parent cluster, as massive stars ($> 40 M_{\odot}$) collapse into BHs before the explosion of such supernovae. Thus, the metallicity measured today is likely higher than the value we should consider in our model, especially for post-starburst galaxies.

4 CONCLUSIONS

Low-metallicity ($Z \lesssim 0.4 Z_{\odot}$) massive ($\gtrsim 40 M_{\odot}$) stars are expected to produce massive remnants ($25 \leq m_{\text{BH}}/M_{\odot} \leq 80$, H03, B10) at the end of their evolution. Such massive BHs might power a large fraction of the observed ULXs in low-metallicity galaxies. In this Paper, we derived the number of massive BHs (N_{BH}) that are expected to form in a galaxy, via this mechanism, in the same time period that they could have a massive ($\gtrsim 15 M_{\odot}$) donor companion. We find that N_{BH} correlates well with the observed number of ULXs per galaxy (N_{ULX}). The slope of such correlation does not depend significantly either on the IMF or on the adopted stellar evolution model. The IMF and the stellar-evolution models affect only the normalization of N_{BH} (the spread is generally less than a factor of 2). We stress that the stellar-evolution models adopted in this Paper neglect some important effects, such as the rotation and the possible influence of binary evolution. The final mass of the remnant is likely affected by the fact that the massive progenitor of the BH is fast rotating or that it resides in a binary, where additional mass loss is possible (see e.g. H03). Accounting for the probability that the progenitor of the massive BH is in a binary system likely introduces additional uncertainties.

In addition, the model considered here does not in-

⁷ The importance of the SFR is somewhat amplified by the larger spread in the SFR values with respect to the metallicity ones.

clude the possibility of pair instability supernovae (PISNs). PISNs are predicted to occur at very low metallicity, in the case of very massive stars ($\geq 140 M_{\odot}$), and lead to the complete disruption of the star (HW02; H03). Pulsational pair instability may occur also for smaller stellar masses ($100 - 140 M_{\odot}$) and/or for larger metallicity, but it does not lead to a PISN, and a massive BH can form via direct collapse. Thus, PISNs probably do not play a role for stars with metallicity $Z \gtrsim 0.01 Z_{\odot}$ and mass $< 140 M_{\odot}$ (H03). On the other hand, even assuming (as a strong upper limit) that all stars with mass $\geq 100 M_{\odot}$ do not leave any remnant, due to a PISN, our estimates of N_{BH} change by less than 10 per cent.

The model described in this Paper is consistent with the observed correlation between the number of ULXs and the SFR, as well as with the fact that ULXs are found preferentially in low-metallicity environments. Furthermore, this model is a natural extension of the scenario described by Grimm et al. (2003). In fact, Grimm et al. (2003) find a correlation between the SFR and the number of X-ray sources (not necessarily ULXs) per galaxy, and they explain it with the correlation between the SFR and the number of HMXBs powered by stellar BHs. In this Paper we suggest that this correlation still holds for the ULXs, as the ULXs (or most of them) can be powered by massive BHs formed by the collapse of massive metal-poor stars.

Our model predicts the existence of a dependence of N_{ULX} on Z (and the data suggest it, too), when the dominant effect due to the SFR is removed. Unfortunately, the statistical uncertainty of such dependence is still quite high, due to the dearth and to the inhomogeneity of the data.

In particular, there is a large inhomogeneity in the metallicity measurements. Moreover, the metallicity needed in our model is that of the molecular clouds before the pollution from the first supernovae associated with the parent clusters, as very massive stars collapse into BHs before such supernovae. Thus, the metallicity measured today is likely higher than the value we should consider in our model. Only for some types of galaxies, such as the ring galaxies, where the star-formation history has a clear connection with the geometry of the system, is it possible to measure a pre-starburst value of Z , suitable for our purposes. A possible way to reduce this problem and to check our model is to take new measurements of the local metallicity in the neighbourhoods of the observed ULXs, or even in the nebula associated with the ULXs (Ripamonti et al., in preparation).

ACKNOWLEDGMENTS

We thank A. Wolter, G. Trinchieri, F. Pizzolato, R. Decarli, G. Ghirlanda, and P. Marigo for useful discussions. We thank the referee for his/her critical reading of the manuscript. MM acknowledges support from the Swiss National Science Foundation, project number 200020-109581/1 and from the Forschungskredit Fellowship 2008 of the University of Zürich. MC and LZ acknowledge financial support from INAF through grant PRIN-2007-26. AB acknowledges ASI INAF contract ASI-INAF I/016/07/0. This research has made use of NASA's Astrophysics Data System Bibliographic Services, of the NASA/IPAC Extragalactic Database (NED; which is operated by the Jet Propulsion

Laboratory, California Institute of Technology, under contract with the National Aeronautics and Space Administration), and of data obtained from the High Energy Astrophysics Science Archive Research Center (HEASARC; which is provided by NASA's Goddard Space Flight Center).

REFERENCES

- Appleton P. N., Marston A. P., 1997, *AJ*, 113, 201
 Begelman M. C., 2002, *ApJ*, 568L, 97
 Belczynski K., Bulik T., Fryer C. L., Ruiter A., Valsecchi F., Vink J. S., Hurley J. R., 2010, *ApJ*, accepted, arXiv:0904.2784 (B10)
 Bell E. F., 2003, *ApJ*, 586, 794
 Bell E. F., Kennicutt R. C. Jr., 2001, *ApJ*, 548, 681
 Bertola F., Bressan A., Burstein D., Buson L. M., Chiosi C., di Serego Alighieri S., 1995, *ApJ*, 438, 680
 Bevington P. R., 1969, *Data reduction and error analysis for the physical sciences*, New York: McGraw-Hill
 Blecha L., Ivanova N., Kalogera V., Belczynski K., Fregeau J., Rasio F., 2006, *ApJ*, 642, 427 (B06)
 Brassington N. J., Read A. M., Ponman T. J., 2005, *MNRAS*, 360, 801
 Brassington N. J., Ponman T. J., Read A. M., 2007, *MNRAS*, 377, 1439
 Bressan A., Fagotto F., Bertelli G., Chiosi C., 1993, *A&AS*, 100, 647
 Buat V., Boselli A., Gavazzi G., Bonfanti C., 2002, *A&A*, 383, 801
 Cash W., 1979, *ApJ*, 228, 939
 Castro-Tirado A. J., Brandt S., Lund N., 1992, *IAU Circ.*, 5590, 2. Edited by Green D. W. E.
 Clemens M. S., Alexander P., Green D. A., 1999, *MNRAS*, 307, 481
 Colbert E. J. M., Petre R., Schlegel E. M., Ryder S. D., 1995, *ApJ*, 446, 177
 Colbert E. J. M., Heckman T. M., Ptak A. F., Strickland D. K., Weaver K. A., 2004, *ApJ*, 602, 231
 Condon J. J., Cotton W. D., Broderick J. J., 2002, *AJ*, 124, 675
 Copperwheat C., Cropper M., Soria R., Wu K., 2007, *MNRAS*, 376, 1407
 Corwin H. G. Jr., Buta R. J., de Vaucouleurs G., 1994, *AJ*, 108, 2128
 Cropper M., Soria R., Mushotzky R. F., Wu K., Markwardt C. B., Pakull M., 2004, *MNRAS*, 349, 39
 D'Agostini G., 2005, arXiv:physics/0511182
 Daflon S., Cunha K., 2004, *ApJ*, 617, 1115
 Deegan P., Combet C., Wynn G. A., 2009, *MNRAS*, in press, arXiv:0908.2566
 de Vaucouleurs G., de Vaucouleurs A., Corwin H. G. Jr., Buta R. J., Paturel G., Fouque P., 1991, *Third Reference Catalogue of Bright Galaxies*, Springer-Verlag Berlin Heidelberg New York
 Dewangan G. C., Miyaji T., Griffiths R. E., Lehmann I., 2004, *ApJ*, 608L, 57
 Dickey J. M., Lockman F. J., 1990, *ARA&A*, 28, 215 [DL90]
 Dopita M. A., Ryder S. D., 1994, *ApJ*, 430, 163
 Dors O. L. Jr., Copetti M. V. F., 2005, *A&A*, 437, 837
 Edmunds M. G., Pagel B. E. J., 1984, *MNRAS*, 211, 507
 Eldridge J. J., Tout C. A., 2004, *MNRAS*, 353, 87
 Eldridge J. J., Vink J. S., 2006, *A&A*, 452, 295
 Fabbiano G., Zezas A., Murray S. S., 2001, *ApJ*, 554, 1035
 Fabbiano G., Baldi A., King A. R., Ponman T. J., Raymond J., Read A., Rots A., Schweizer F., Zezas A., 2004, *ApJ*, 605L, 21
 Fagotto F., Bressan A., Bertelli G., Chiosi C., 1994a, *A&AS*, 105, 29

- Fagotto F., Bressan A., Bertelli G., Chiosi C., 1994b, *A&AS*, 105, 39
- Fender R., Belloni T., 2004, *ARA&A*, 42, 317
- Fosbury R. A. E., Hawarden T. G., 1977, *MNRAS*, 178, 473
- French, H. B., 1980, *ApJ*, 240, 41
- Fryer C. L., 1999, *ApJ*, 522, 413
- Garnett D. R., 1990, *ApJ*, 363, 142
- Gavazzi G., Boselli A., Pedotti P., Gallazzi A., Carrasco L., 2002, *A&A*, 396, 449
- Gehrels N., 1986, *ApJ*, 303, 336
- Gil de Paz A., Madore B. F., Pevunova O., 2003, *ApJS*, 147, 29
- Gilfanov M., Grimm H.-J., Sunyaev R., 2004a, *MNRAS*, 347L, 57
- Gilfanov M., Grimm H.-J., Sunyaev R., 2004b, *Nuclear Physics B Proceedings Supplements*, 132, 369
- Gilfanov M., Grimm H.-J., Sunyaev R., 2004c, *MNRAS*, 351, 1365
- Gonçalves A. C., Soria R., 2006, *MNRAS*, 371, 673
- Gonzalez-Delgado R. M., Perez E., Diaz A. I., Garcia-Vargas M. L., Terlevich E., Vilchez J. M., 1995, *ApJ*, 439, 604
- Grimm H.-J., Gilfanov M., Sunyaev R., 2002, *A&A* 391, 923
- Grimm H.-J., Gilfanov M., Sunyaev R., 2003, *MNRAS*, 339, 793
- Guseva N. G., Izotov Y. I., Thuan T. X., 2000, *ApJ*, 531, 776
- Harlaftis E. T., Greiner J., 2004, *A&A*, 414L, 13
- Hasinger G., Burg R., Giacconi R., Schmidt M., Trümper J., Zamorani G., 1998, *A&A*, 329, 482
- Hawley S. A., Phillips M. M., 1980, *ApJ*, 235, 783
- Heger A., Fryer C.L., Woosley S.E., Langer N., Hartmann D.H., 2003, *ApJ*, 591, 288 (H03)
- Heger A., Woosley S.E., 2002, *ApJ*, 567, 532 (HW02)
- Helou G., et al., 2004, *ApJS*, 154, 253
- Helmboldt J. F., Walterbos R. A. M., Bothun G. D., O'Neil K., de Blok W. J. G., 2004, *ApJ*, 613, 914
- Hirashita H., Buat V., Inoue A. K., 2003, *A&A*, 410, 83
- Hopkins A. M., Schulte-Ladbeck R. E., Drozdovsky I. O., 2002, *AJ*, 124, 862
- Hunter D. A., Elmegreen B. G., 2004, *AJ*, 128, 2170
- Iglesias-Páramo J., et al., 2006, *ApJS*, 164, 38
- Irwin J. A., Sarazin C. L., Bregman J. N., 2002, *ApJ*, 570, 152
- Irwin J. A., Bregman J. N., Athey A. E., 2004, *ApJ*, 601L, 143
- Izotov Y. I., Thuan T. X., Lipovetsky V. A., 1997, *ApJS*, 108, 1
- Kaaret P., 2001, *ApJ*, 560, 715
- Kaaret P., Alonso-Herrero A., 2008, *ApJ*, 682, 1020
- Kaaret P., Ward M. J., Zezas A., 2004, *MNRAS*, 351L, 83
- Kehrig C., Telles E., Cuisinier F., 2004, *AJ*, 128, 1141
- Kennicutt R. C. Jr., Kent, S. M., 1983, *AJ*, 88, 1094
- Kennicutt R. C. Jr., Roettiger K. A., Keel W. C., van der Hulst J. M., Hummel E., 1987, *AJ*, 93, 1011
- Kennicutt R. C. Jr., 1992, *ApJ*, 388, 310
- Kennicutt R. C. Jr., Tamblyn P., Congdon C. E., 1994, *ApJ*, 435, 22
- Kennicutt R. C. Jr., 1998, *ApJ*, 498, 541 [K98]
- Kennicutt R. C. Jr., Bresolin F., Garnett D. R., 2003, *ApJ*, 591, 801
- Kewley L. J., Geller M. J., Jansen R. A., Dopita M. A., 2002, *AJ*, 124, 3135
- Kewley L. J., Jansen R. A., Geller M. J., 2005, *PASP*, 117, 227
- King A. R., Davies M. B., Ward M. J., Fabbiano G., Elvis M., 2001, *ApJL*, 552, 109
- King A. R., Pounds K. A., 2003, *MNRAS*, 345, 657
- King A. R., 2008, *MNRAS*, 385L, 113
- Kroupa P., 2001, *MNRAS*, 322, 231
- Lee H., Skillman E. D., 2004, *ApJ*, 614, 698
- Legrand F., Tenorio-Tagle G., Silich S., Kunth D., Cerviño M., 2001, *ApJ*, 560, 630
- Liu J.-F., Bregman J. N., 2005, *ApJS*, 157, 59 (LB05)
- Liu Q. Z., Mirabel I. F., 2005, *A&A*, 429, 1125 (LM05)
- Liu J.-F., Bregman J. N., Irwin J., 2006, *ApJ*, 642, 171
- Long K.S., Helfand D.J., Grabelsky D.A., 1981, *ApJ*, 248, 925
- Lonsdale C. J., Helou G., 1985, *Cataloged Galaxies and Quasars Observed in the IRAS Survey*, Pasadena: Jet Propulsion Laboratory (JPL)
- López-Corredoira M., Gutiérrez C. M., 2006, *A&A*, 454, 77
- Maeder A., 1992, *A&A*, 264, 105 (M92)
- Mapelli M., Colpi M., Zampieri L., 2009, *MNRAS*, 395L, 71 (Paper I)
- Martin C. L., 1997, *ApJ*, 491, 561
- Martin P., Friedli D., 1997, *A&A*, 326, 449
- Masegosa J., Moles M., Campos-Aguilar A., 1994, *ApJ*, 420, 576
- Mayya Y. D., Bizyaev D., Romano R., Garcia-Barreto J. A., Vorobyov E. I., 2005, *ApJ*, 620L, 35
- Miller B. W., Hodge P., 1994, *ApJ*, 427, 656
- Miller B. W., Hodge P., 1996, *ApJ*, 458, 467
- Moustakas J., Kennicutt R. C., Jr., 2006a, *ApJ*, 651, 155
- Moustakas J., Kennicutt R. C., Jr., 2006b, *ApJS*, 164, 81
- Muñoz-Mateos J. C., Gil de Paz A., Boissier S., Zamorano J., Jarrett T., Gallego J., Madore B. F., 2007, *ApJ*, 658, 1006
- Mushotzky R., 2004, *Progress of Theoretical Physics Supplement*, 155, 27
- Oliva E., Marconi A., Moorwood A. F. M., 1999, *A&A*, 342, 870
- Orosz J. A., 2003, in van der Hucht K. A., Herrero A., Esteban, C., eds, *Proc. IAU Symp. 212, A Massive Star Odyssey: From Main Sequence to Supernova*
- Pagel B. E. J., Simonson E. A., Terlevich R. J., Edmunds M. G., 1992, *MNRAS*, 255, 325
- Pakull M. W., Mirioni L., 2002, *astro-ph/0202488*
- Pastoriza M. G., Dottori H. A., Terlevich E., Terlevich R., Diaz A. I., 1993, *MNRAS*, 260, 177
- Patruno A., Colpi M., Faulkner A., Possenti A., 2005, *MNRAS*, 364, 344
- Pilyugin L. S., 2001a, *A&A*, 369, 594 [P01]
- Pilyugin L. S., 2001b, *A&A*, 374, 412
- Pilyugin L. S., Izotova I. Yu., Sholudchenko Yu. S., 2008, *Kinematics and Physics of Celestial Bodies*, 24, 192
- Pilyugin L. S., Mollá M., Ferrini F., Vilchez J. M., 2002, *A&A*, 383, 14
- Pilyugin L. S., Thuan T. X., 2005, *ApJ*, 631, 231 [PT05]
- Pilyugin L. S., Thuan T. X., 2007, *ApJ*, 669, 299
- Pilyugin L. S., Vilchez J. M., Contini T., 2004, *A&A*, 425, 849 [PVC04]
- Pilyugin L. S., Thuan T. X., Vilchez J. M., 2006, *MNRAS*, 367, 1139
- Portegies Zwart S. F., Dewi J., Maccarone T. 2004, *MNRAS*, 355, 413
- Portinari L., Chiosi C., Bressan A., 1998, *A&A*, 334, 505 (P98)
- Poutanen J., Lipunova G., Fabrika S., Butkevich A. G., Abolmasov P., 2007, *MNRAS*, 377, 1187
- Ptak A., Colbert E., 2004, *ApJ*, 606, 291
- Ranalli P., Comastri A., Setti G., 2003, *A&A*, 399, 39
- Read A. M., 2003, *MNRAS*, 342, 715
- Roberts T. P., 2007, *Astrophysics and Space Science*, 311, 203
- Ryder S. D., Dopita M. A., 1994, *ApJ*, 430, 142
- Salpeter E. E., 1955, *ApJ*, 121, 161
- Schmitt H. R., Calzetti D., Armus L., Giavalisco M., Heckman T. M., Kennicutt R. C. Jr., Leitherer C., Meurer G. R., 2006, *ApJ*, 643, 173
- Skillman E. D., Kennicutt R. C., Hodge P. W., 1989, *ApJ*, 347, 875
- Smith B. J., Struck C., Nowak M. A., 2005, *AJ*, 129, 1350
- Smith D. A., Wilson A. S., 2001, *ApJ*, 557, 180
- Socrates A., Davis S. W., 2006, *ApJ*, 651, 1049
- Soria R., Cropper M., Pakull M., Mushotzky R., Wu K., 2005, *MNRAS*, 356, 12
- Spinoglio L., Andreani P., Malkan M. A., 2002, *ApJ*, 572, 105
- Stevens I. R., Forbes D. A., Norris R. P., 2002, *MNRAS*, 335, 1079
- Stobbart A.-M., Roberts T. P., Wilms J., 2006, *MNRAS*, 368, 397
- Strateva I. V., Komossa S., 2009a, *ApJ*, 692, 443

- Strateva I. V., Komossa S., 2009b, MNRAS, submitted, arXiv:0903.1548
- Strohmayer T. E., Mushotzky R. F., 2003, ApJ, 586L, 61
- Strohmayer T. E., Mushotzky R. F., Winter L., Soria R., Uttley P., Cropper M., 2007, ApJ, 660, 580
- Swartz D. A., Ghosh K. K., Tennant A. F., Wu K., 2004, ApJS, 154, 519
- Swartz D. A., Soria R., Tennant A. F., 2008, ApJ, 684, 282
- Trinchieri G., Fabbiano G., Bandiera R., 1989, ApJ, 342, 759
- Tschöke D., Hensler G., Junkes N., 2000, A&A, 360, 447
- van der Marel R. P., 2004, in Ho L., ed., *Coevolution of Black Holes and Galaxies*, Cambridge Univ. Press, p. 37
- Vigroux L., Stasińska G., Comte G., 1987, A&A, 172, 15
- Walter F., et al., 2007, ApJ, 661, 102
- Wang Q. D., Whitaker K. E., Williams R., 2005, MNRAS, 362, 1065
- Wang Q., Wu X., 1992, ApJS, 78, 391
- Webster B. L., Smith M. G., 1983, MNRAS, 204, 743
- Winter L. M., Mushotzky R. F., Reynolds C. S., 2006, ApJ, 649, 730
- Wolter A., Trinchieri G., 2004, A&A, 426, 787
- Woosley S. E., Weaver T. A., 1986, ARA&A, 24, 205
- Zampieri L., Mucciarelli P., Falomo R., Kaaret P., Di Stefano R., Turolla R., Chierigato M., Treves A., 2004, ApJ, 603, 523
- Zampieri L., Roberts T., 2009, MNRAS, 400, 677

APPENDIX A: COMPARISON BETWEEN KROUPA AND SALPETER IMF

In this paper we assumed the Kroupa IMF (Kroupa 2001), a moderately top-heavy IMF. In this Appendix we show how sensitive our model is to the adopted IMF, by using the Salpeter IMF (Salpeter 1995) to derive N_{BH} . Table A1 and Fig. A1 show the results obtained adopting the Salpeter IMF. Basically, all the values of N_{BH} calculated with the Salpeter IMF are a factor of 2 lower than the ones obtained with the Kroupa IMF. However, the slope of the fit in equation (5) does not change significantly with a different IMF. Adopting the Salpeter IMF (Fig. A1), for the fits in equation (5) we find $\beta = 0.80^{+0.16}_{-0.12}$ ($\beta = 0.85^{+0.19}_{-0.13}$) and $\gamma = -2.12^{+0.43}_{-0.56}$ ($\gamma = -2.50^{+0.49}_{-0.70}$), corresponding to $\chi^2 = 8.7$ ($\chi^2 = 11.1$) with 62 dof, for the models by P98 (B10). As for the Kroupa IMF, fixing $\beta = 1$, we still obtain good values of χ^2 ($\chi^2 = 10.0$ and 11.7 with 63 dof, for P98 and B10, respectively). Thus, only the normalization of N_{BH} is affected by a different choice of the IMF.

APPENDIX B: DATA COLLECTION AND ELABORATION

In this section we provide details about how we collected and calculated the values reported in Table 1, that represent the observational basis of this paper.

B1 Star Formation Rate

As we already mentioned, the SFR reported in Tables 1 comes from either ultra-violet (UV), $\text{H}\alpha$, far-infrared (FIR), or radio measurements. If more than one independent measurement is available, we generally average the corresponding SFRs, keeping into account the properties of the galaxy, of the observational data, and of calibrations.

In particular, for galaxies included in the UV catalogue by Muñoz-Mateos et al. (2007), we derive $\text{SFR} = 2\pi r_\alpha^2 \Sigma_{\text{SFR0}} [1 - (1 + r_{\text{tot}}/r_\alpha) \exp(-r_{\text{tot}}/r_\alpha)]$, where Σ_{SFR0} is the central SFR surface density, r_α is a characteristic length-scale and r_{tot} is the external radius of the galaxy (from the integration of equation B1a in Muñoz-Mateos et al. 2007). When the total $\text{H}\alpha$ luminosities are available, we adopt the correlation in Kennicutt (1998; hereafter K98), i.e. $\text{SFR} = L(\text{H}\alpha)/1.26 \times 10^{41} \text{ erg s}^{-1} [\text{M}_\odot \text{ yr}^{-1}]$. Similarly, when the FIR luminosity is available, we apply the equation $\text{SFR} = L(\text{FIR})/2.2 \times 10^{43} \text{ erg s}^{-1} [\text{M}_\odot \text{ yr}^{-1}]$ in K98. When a radio measurement (at 1.4 GHz) is available, we then use equation (6) of Bell (2003). Finally, if a galaxy belongs to the sample by Grimm et al. (2003), we generally use their adopted values.

B2 Metallicity

The existence of a metallicity measurement is the most restrictive among the criteria for inclusion in our sample, as metallicities are often unavailable.

For most galaxies in the sample we use measurements of oxygen abundance (based on oxygen line intensities from HII regions) as proxies for metallicity. Instead, when the spectra of HII regions are unavailable, we use X-ray metallicity estimates (from papers on X-ray measurements of ULXs), although they are much less accurate. In the rest of this subsection we provide extra details about the measurements from HII regions.

B2.1 Conversion of line intensities to metallicities

When line intensity measurements include the weak $\lambda=4363\text{\AA}$ OIII line (e.g. in the case of HII regions of the Cartwheel galaxy from Fosbury & Hawarden 1979), we simply use the oxygen abundances reported in the literature: this is possible because the measurement of the 4363\AA line greatly simplifies the conversion of line intensities into abundances, and the conversion procedure did not change much since it was first established (see e.g. Pagel et al. 1992; and the discussion in PT05). Instead, when only the most intense OII ($\lambda=3727\text{\AA}$) and OIII ($\lambda=4959, 5007\text{\AA}$) lines are observed, the oxygen abundances in different papers are often based on different calibrations (see the discussion in P01, and in PT05), that lead to significant offsets in the results. For this reason, we went back to the observational data and applied the PT05 calibration whenever this was possible. We made an exception for galaxies where the metallicity value in the literature had been calculated with the P01 calibration (such as the ones in the compilation by Pilyugin, Vílchez & Contini 2004; hereafter PVC04); this is because the two calibrations are quite close to each other (the PT05 calibration is essentially a revision of the P01 calibration), and the difference (typically amounting to ~ 0.05 dex for single HII regions; see the top panel of Fig. 7 from PT05) should not have a large effect.

We note that both the PT05, and the P01 calibrations generally provide significantly lower abundances with respect to previous calibrations (e.g. Edmunds & Pagel 1984), but are currently considered the most accurate (see e.g. Kennicutt, Bresolin & Garnett 2003, who actually suggest that abundances might be even lower).

Table A1. Values of N_{BH} and ϵ_{BH} for the galaxies listed in Table 1, assuming the models by P98 (first and second column) and by B10 (third and fourth column). We adopt a Salpeter IMF.

Galaxy	N_{BH} (P98)	$\epsilon_{\text{BH}}/10^{-4}$ (P98)	N_{BH} (B10)	$\epsilon_{\text{BH}}/10^{-4}$ (B10)
The Cartwheel	20600^{+10700}_{-10600}	$9.2^{+5.5}_{-5.2}$	34600^{+17400}_{-17500}	$5.5^{+3.2}_{-3.0}$
NGC 253	2970^{+1560}_{-1590}	$10.0^{+11.1}_{-7.7}$	5490^{+2830}_{-2930}	$5.4^{+6.0}_{-4.1}$
NGC 300	120^{+61}_{-64}	$0^{+152.5}_{-0}$	216^{+109}_{-111}	$0^{+84.7}_{-0}$
NGC 598	626^{+348}_{-626}	$16.0^{+37.6}_{-16.0}$	1230^{+650}_{-680}	$8.1^{+19.1}_{-8.1}$
NGC 628	1400^{+770}_{-760}	$13.7^{+20.2}_{-12.0}$	2680^{+1420}_{-1400}	$7.2^{+10.5}_{-6.2}$
NGC 1058	185^{+97}_{-100}	$49.2^{+126.5}_{-49.2}$	349^{+184}_{-182}	$26.1^{+67.0}_{-26.1}$
NGC 1073	632^{+356}_{-632}	$31.6^{+45.3}_{-31.6}$	1280^{+680}_{-710}	$15.6^{+22.1}_{-13.2}$
NGC 1291	1340^{+670}_{-680}	$21.6^{+21.2}_{-16.5}$	1820^{+920}_{-910}	$15.9^{+17.5}_{-12.1}$
NGC 1313	1700^{+860}_{-860}	$11.7^{+16.5}_{-9.6}$	2520^{+1270}_{-1260}	$7.9^{+11.2}_{-6.5}$
NGC 1365	6190^{+3150}_{-3280}	$13.2^{+9.5}_{-8.6}$	10280^{+5420}_{-5200}	$11.8^{+7.8}_{-7.0}$
IC 342	412^{+222}_{-213}	$48.1^{+68.9}_{-40.2}$	741^{+375}_{-379}	$26.7^{+38.0}_{-22.2}$
NGC 1566	1740^{+970}_{-1740}	$14.4^{+21.0}_{-14.4}$	3330^{+1840}_{-1750}	$7.5^{+11.0}_{-7.9}$
NGC 1705	75^{+38}_{-40}	$0^{+244.0}_{-0}$	135^{+68}_{-70}	$0^{+135.6}_{-0}$
NGC 2366	91^{+46}_{-47}	$0^{+201.1}_{-0}$	134^{+68}_{-67}	$0^{+136.6}_{-0}$
NGC 2403	312^{+163}_{-166}	$32.0^{+75.3}_{-31.6}$	571^{+294}_{-298}	$17.5^{+41.1}_{-17.2}$
NGC 2442	0^{+2580}_{-0}	> 2.6	2900^{+2150}_{-2900}	$2.3^{+10.0}_{-2.3}$
Holmberg II	122^{+62}_{-62}	$82.0^{+192.2}_{-79.7}$	180^{+91}_{-90}	$55.6^{+130.3}_{-53.9}$
NGC 2903	1190^{+660}_{-670}	$16.0^{+23.7}_{-14.2}$	2280^{+1210}_{-1190}	$8.4^{+12.3}_{-7.3}$
NGC 3031	2100^{+1160}_{-1140}	$9.4^{+13.5}_{-8.0}$	4020^{+2130}_{-2110}	$4.9^{+7.0}_{-4.1}$
NGC 3049	0^{+0}_{-0}	—	0^{+0}_{-0}	—
PGC 30819	54^{+27}_{-28}	$0^{+338.9}_{-0}$	92^{+47}_{-47}	$0^{+198.9}_{-0}$
NGC 3310	1720^{+930}_{-920}	$16.5^{+19.1}_{-13.2}$	3140^{+1620}_{-1640}	$9.0^{+10.4}_{-7.1}$
NGC 3395/3396	3670^{+1980}_{-1960}	$19.1^{+14.5}_{-12.4}$	6710^{+3460}_{-3440}	$10.4^{+7.8}_{-6.6}$
PGC 35286	24^{+12}_{-12}	$0^{+762.5}_{-0}$	34^{+17}_{-17}	$0^{+538.2}_{-0}$
PGC 35684	12^{+6}_{-6}	$0^{+1525.0}_{-0}$	19^{+10}_{-10}	$0^{+963.2}_{-0}$
NGC 3738	31^{+16}_{-17}	$0^{+590.3}_{-0}$	56^{+28}_{-29}	$0^{+326.8}_{-0}$
NGC 3972	152^{+85}_{-152}	$0^{+120.4}_{-0}$	308^{+164}_{-171}	$0^{+59.4}_{-0}$
Antennae	11000^{+5500}_{-5500}	$13.7^{+8.2}_{-7.8}$	14800^{+7400}_{-7400}	$10.1^{+6.1}_{-5.7}$
NGC 4144	41^{+21}_{-22}	$0^{+446.3}_{-0}$	74^{+37}_{-38}	$0^{+247.3}_{-0}$
NGC 4214	105^{+56}_{-55}	$0^{+174.3}_{-0}$	199^{+101}_{-104}	$0^{+92.0}_{-0}$
NGC 4236	94^{+49}_{-50}	$0^{+194.7}_{-0}$	171^{+87}_{-89}	$0^{+107.0}_{-0}$
NGC 4248	12^{+7}_{-6}	$0^{+1525.0}_{-0}$	24^{+12}_{-13}	$0^{+762.5}_{-0}$
NGC 4254	2690^{+1410}_{-1450}	$6.0^{+12.1}_{-6.0}$	5280^{+2720}_{-2760}	$3.0^{+6.1}_{-3.0}$
NGC 4258	1420^{+790}_{-1420}	$17.0^{+22.9}_{-17.0}$	2790^{+1480}_{-1540}	$8.7^{+11.6}_{-8.0}$
NGC 4303	4750^{+2480}_{-2530}	$8.6^{+9.2}_{-7.4}$	8280^{+4370}_{-4190}	$4.9^{+5.3}_{-4.1}$
NGC 4321	3060^{+1680}_{-1650}	$16.7^{+16.0}_{-13.2}$	5840^{+3090}_{-3060}	$8.8^{+8.3}_{-6.8}$
NGC 4395	97^{+52}_{-52}	$99.0^{+242.1}_{-99.0}$	177^{+91}_{-92}	$54.2^{+132.4}_{-54.2}$
NGC 4449	200^{+105}_{-107}	$0^{+91.5}_{-0}$	373^{+197}_{-195}	$0^{+49.1}_{-0}$
NGC 4485/4490	3370^{+1760}_{-1800}	$14.5^{+12.6}_{-10.1}$	6220^{+3200}_{-3250}	$7.9^{+6.8}_{-5.4}$
NGC 4501	0^{+1550}_{-0}	> 8.3	0^{+3300}_{-0}	> 3.9
NGC 4559	1160^{+610}_{-620}	$17.2^{+24.3}_{-14.4}$	2090^{+1060}_{-1090}	$9.6^{+13.5}_{-7.9}$
NGC 4631	2180^{+1180}_{-1160}	$8.4^{+12.9}_{-7.7}$	3980^{+2050}_{-2080}	$4.6^{+7.0}_{-4.2}$
NGC 4651	1020^{+550}_{-530}	$8.1^{+22.9}_{-8.1}$	1960^{+990}_{-1020}	$4.2^{+11.9}_{-4.2}$
NGC 4656	1250^{+630}_{-630}	$7.6^{+18.7}_{-7.6}$	1840^{+920}_{-920}	$5.2^{+12.7}_{-5.2}$
The Mice	3420^{+1200}_{-3420}	$17.6^{+14.3}_{-17.6}$	6720^{+3690}_{-3530}	$8.9^{+7.2}_{-5.9}$
NGC 4736	945^{+481}_{-501}	$9.0^{+24.7}_{-9.0}$	1630^{+840}_{-840}	$5.2^{+14.3}_{-5.8}$
NGC 4861	638^{+330}_{-328}	$29.6^{+44.0}_{-25.8}$	1030^{+520}_{-520}	$18.4^{+27.2}_{-15.9}$
PGC 45561	0^{+184}_{-0}	$0^{+99.5}_{-0}$	260^{+145}_{-260}	$0^{+70.4}_{-0}$
NGC 5033	1990^{+1010}_{-1000}	$6.8^{+14.0}_{-6.8}$	2930^{+1470}_{-1470}	$4.6^{+9.5}_{-4.6}$
NGC 5055	996^{+553}_{-996}	$18.3^{+28.3}_{-18.3}$	1960^{+1040}_{-1030}	$9.3^{+14.3}_{-8.5}$
NGC 5194/5195	0^{+8470}_{-0}	> 10.5	11400^{+6700}_{-11400}	$7.8^{+5.8}_{-7.8}$
NGC 5236	0^{+1750}_{-0}	> 5.2	2450^{+1310}_{-1780}	$3.7^{+9.6}_{-3.7}$
NGC 5238	9^{+5}_{-5}	$0^{+2033.0}_{-0}$	17^{+9}_{-9}	$0^{+1076.0}_{-0}$
NGC 5408	109^{+55}_{-55}	$91.7^{+215.2}_{-89.2}$	162^{+82}_{-81}	$61.7^{+144.8}_{-59.8}$
NGC 5457	2890^{+1470}_{-1530}	$22.8^{+17.5}_{-15.1}$	4740^{+2400}_{-2400}	$13.9^{+10.6}_{-9.0}$

Table A1 - continued.

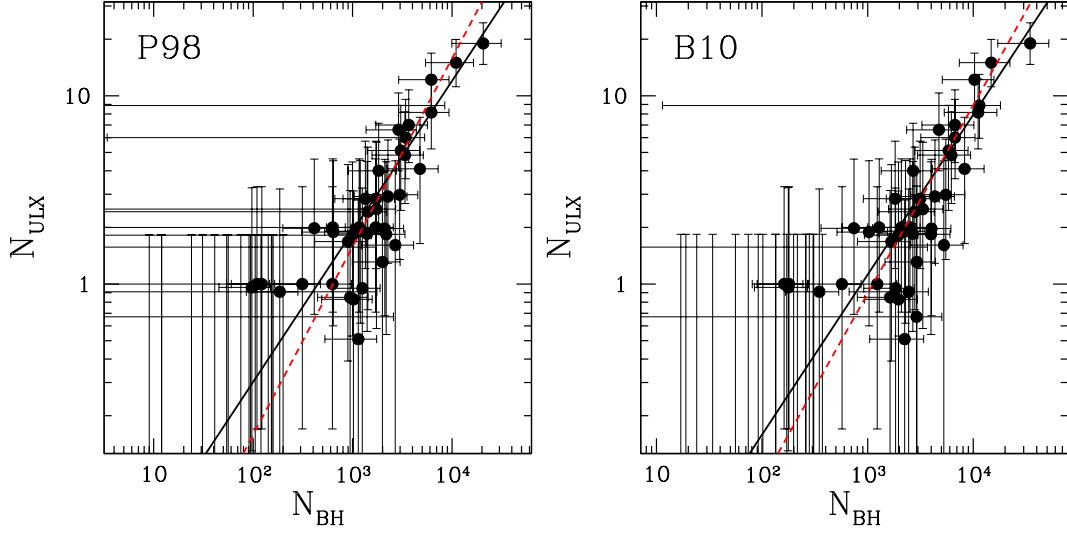


Figure A1. Number of expected massive BHs per galaxy, derived using the models from P98 (left-hand panel) and from B10 (right-hand panel), versus the number of observed ULXs per galaxy. The adopted IMF is a Salpeter IMF. The filled circles are the galaxies listed in Table 1. The error bars on both the x - and the y - axis are $1 - \sigma$ errors. The error bars on N_{BH} account for the uncertainty on the SFR and on the metallicity (see Section 2.3 for details). The solid lines are the power-law fits, for the entire sample. The dashed lines (red on the web) are the power-law fits.

Table A1 - continued.

Galaxy	N_{BH} (P98)	$\epsilon_{\text{BH}}/10^{-4}$ (P98)	N_{BH} (B10)	$\epsilon_{\text{BH}}/10^{-4}$ (B10)
Circinus	1820^{+920}_{-920}	$21.9^{+20.5}_{-15.2}$	2700^{+1360}_{-1350}	$14.8^{+13.9}_{-10.3}$
NGC 6946	2270^{+1250}_{-1230}	$12.9^{+14.6}_{-10.1}$	4340^{+2300}_{-2270}	$6.7^{+7.6}_{-5.2}$
PGC 68618	1140^{+600}_{-610}	$4.5^{+20.6}_{-4.5}$	2240^{+1160}_{-1200}	$2.3^{+10.5}_{-2.3}$
NGC 7714/7715	6190^{+3150}_{-3280}	$19.7^{+12.6}_{-12.0}$	11100^{+5600}_{-5800}	$7.3^{+5.3}_{-4.7}$
NGC 7742	898^{+489}_{-482}	$18.7^{+31.2}_{-18.6}$	1680^{+880}_{-880}	$10.0^{+16.7}_{-9.9}$
Milky Way	142^{+79}_{-142}	$0^{+128.9}_{-0}$	280^{+149}_{-147}	$0^{+65.4}_{-0}$
IC 10	56^{+30}_{-30}	$0^{+326.8}_{-0}$	102^{+53}_{-53}	$0^{+179.4}_{-0}$
LMC	159^{+87}_{-86}	$0^{+115.1}_{-0}$	304^{+161}_{-159}	$0^{+60.2}_{-0}$
SMC	154^{+82}_{-78}	$0^{+118.8}_{-0}$	260^{+130}_{-130}	$0^{+70.4}_{-0}$

When the metallicity gradient is available for a given galaxy, we list in Table 1 and adopt in our calculations the value of the metallicity at $r = 0.73 R_{25}$, where R_{25} is the isophotal or Holmberg radius. In fact, $r = 0.73 R_{25}$ is the average distance of the observed ULXs from the centre of the host galaxy, in a sample of spiral galaxies (fig. 15 in Liu et al. 2006; the averaging process took contamination into account).

The oxygen abundance is usually derived in terms of $12 + \log(\text{O}/\text{H})$; this can be easily converted to the units used in Table 1 (where the metallicity Z is expressed as a fraction of solar metallicity Z_{\odot}), by assuming that $12 + \log(\text{O}/\text{H})_{\odot} = 8.92$, which corresponds to $Z_{\odot} = 0.02$ (the value commonly used in stellar evolution studies).

B3 Distance

For the 52 galaxies in the LB05 catalogue we use the distance reported there. For the MW we simply indicate the distance to the Galactic centre (8.5 kpc). For the remaining 11 galaxies we use the distances reported by the NASA

Extragalactic Database (NED). In the 9 cases where it is possible, we take the mean redshift-independent distance; for the remaining 2 galaxies we derive distances from the redshift, assuming $H_0 = 73 \text{ km s}^{-1} \text{ Mpc}^{-1}$.

B4 Contaminating sources

B4.1 Further required data

Estimating the number of contaminating sources requires the use of several quantities that are not reported in Table 1: the galaxy angular size (major and minor axis R_{25} and r_{25} of the 25 mag arcsec $^{-2}$ isophote), the sky area A_{obs} actually covered by the X-ray observations, and the total galactic HI column density (N_{H}).

For galaxies in the LB05 catalogue, we use the R_{25} , r_{25} and N_{H} values reported there. For the others, we adopt the references quoted in LB05: the RC3 catalogue (de Vaucouleurs et al. 1991) for angular sizes, and the paper of Dickey & Lockman (1990; hereafter DL90) for the weighted average of N_{H} . We make an exception for the MW and the

Magellanic Clouds, where such quantities do not really matter, since the number density of the expected contaminating sources is extremely low, and there are no ULXs inside such galaxies.

The sky area A_{obs} was taken from the papers reporting the X-ray observations. When no specific information is provided, we assume an area of 314 arcmin^2 if the data were taken with ROSAT (this corresponds to the area within $10'$ from the instrument's axis, where the sensitivity is reasonably constant and close to the maximum value; see LB05), or an area of 70.6 arcmin^2 (i.e. the entire $8.4' \times 8.4'$ field of view of the S3 detector) if the data were taken with *Chandra*.

B4.2 Contamination estimate

In order to estimate the number of background or foreground contaminating sources, we followed a procedure very similar to the one reported by Liu et al. (2006).

Since the bulk of the galaxies in our sample was observed with ROSAT, we used the $\log(N)\text{-}\log(S)$ reported in Hasinger et al. (1998). We converted the minimum luminosity of an ULX, $L_{\text{lim}} = 10^{39} \text{ erg s}^{-1}$, into the apparent flux limit $F_{\text{lim}} = L_{\text{lim}}/(4\pi D^2)$; then, we converted F_{lim} into another flux S_{lim} that can be used in the Hasinger et al. (1998) $\log(N)\text{-}\log(S)$ relation. Such conversion takes into account (i) the different assumptions on the observed band (the Hasinger et al. 1998 flux refers to the 0.5–2.4 keV band, whereas most references for ULXs provide luminosities in other bands - e.g. 0.3–8.0 keV band); (ii) the different assumption over spectral slopes (Hasinger et al. 1998 assumes that all sources have photon index 2; whereas here we assume a photon index 1.7, as done by LB05); (iii) the absorption from the galactic N_{H} . In most cases, such conversion amounts to a reduction by a factor of 2–3 (the exact value depending on the band used for the X-ray observations, and to a lesser extent on the galactic N_{H} for each specific galaxy) of F_{lim} . Finally, we integrate the Hasinger et al. (1998) differential $\log(N)\text{-}\log(S)$, and find the expected surface number density q of contaminating sources (i.e. of sources with apparent flux larger than S_{lim}).

In order to determine the expected contamination in a specific galaxy, we combined q with the size of the galaxy (and of the observed area), taking into account also the radial distribution of ULXs. The exact procedure is the following. First of all, we calculate the observed area with deprojected distance $\leq R_{25}$ from the centre $A_1 = \min(A_{\text{obs}}, \pi R_{25}^2)$, and the observed area with deprojected distance between R_{25} and $2R_{25}$, $A_2 = \min(A_{\text{obs}} - A_1, \pi R_{25}^2)$. This assumes that the field of the X-ray observation was centred on the host galaxy, and that such field is circular. Then, we obtain the number of expected contaminating sources in the two regions, $Q_1 = A_1 q$ and $Q_2 = A_2 q$. These must be compared to the numbers N_1 and N_2 of observed ULXs in the corresponding areas (obviously, $N_1 + N_2 = N_{\text{ULX, raw}}$), since the number of contaminating sources cannot be larger than the number of observed sources. Then, we estimate the actual number of contaminating sources to be

$$Q = \min(Q_1, N_1) + \min(Q_2, N_2). \quad (\text{B1})$$

This expression automatically sets the number of contaminating sources at 0 for galaxies where no ULX was observed.

For the 10 galaxies where the original X-ray observations provide a value of the number of ULXs that was already cleared from contaminating sources (e.g. because one or more of the candidate ULXs in a galaxy have been identified as background objects), we simply assume that $N_{\text{ULX, raw}} = N_{\text{ULX}}$, i.e. that $Q = 0$.

The total number of expected contaminating sources in the 54 galaxies where we apply our estimates is 14.60, whereas the sum of $N_{\text{ULX, raw}}$ in such galaxies is 112; the contamination fraction is then $\simeq 0.13$, which is smaller than those found in previous papers (25 – 44 per cent, Swartz et al. 2004; Ptak & Colbert 2004; Liu et al. 2006; López-Corredoira & Gutiérrez 2006). There are two reasons for this discrepancy. First, we do not consider elliptical galaxies, where the contamination is stronger: for example, Liu et al. (2006) estimate a contamination fraction ~ 1 for early type galaxies, whereas for late-type galaxy such fraction is only ~ 0.2 . Second, our sample includes a smaller fraction of distant galaxies than most ULXs catalogues (for example, in the LB05 catalogue the fraction of galaxies with distances $\geq 20 \text{ Mpc}$ is ~ 0.4 , whereas in our sample it is $\lesssim 0.1$): this is relevant because distant galaxies tend to have higher contamination levels than nearby galaxies⁸.

B5 A possible contamination from Population II ULXs

ULXs in elliptical galaxies might be connected to the minor (but non-negligible) fraction of ULXs that is claimed (e.g. Colbert et al. 2004; Brassington et al. 2005) to be associated with old stellar populations (Population II ULXs). Since old populations are present also in spiral galaxies, Population II ULXs might be present also in our sample. It is quite difficult to estimate their number.

Liu et al. (2006) estimate that the number of ULXs in early-type and elliptical galaxies can be completely explained by contaminating sources (i.e. without requiring Population II ULXs): if so, the number of ULXs associated to old stellar populations should be very low (or even negligible) also in spiral/irregular galaxies. On the other hand, Colbert et al. (2004) suggest that Population II ULXs represent a fraction ~ 0.2 of ULXs in spirals. However, the results by Colbert et al. (2004) and by Liu et al. (2006) are not necessarily in conflict. In fact, $1\text{-}\sigma$ upper limits for early-type galaxies⁹ from Liu et al. (2006) are not far from the Colbert et al. (2004) results. Since the fraction of population II

⁸ The distance D affects of the contamination Q through the angular surface of a galaxy, and the corresponding limit flux S_{lim} . Both scale as D^{-2} . However, the Hasinger et al. (1998) $\log(N) - \log(S)$ implies that for $D \lesssim 30 \text{ Mpc}$ the decrease in S_{lim} produces a steep increase in the surface density of contaminating sources ($q \propto D^{3.4}$), and $Q \propto D^{1.4}$; instead, for sources at large distances the two dependencies almost cancel out, and $Q \propto D^{-0.1}$.

⁹ In their Section 3.2 and Tables 1 and 2, Liu et al. (2006) estimate the occurrence frequencies of ULXs. They find 0.72 ± 0.11 ULXs per spiral galaxy, 0.02 ± 0.11 ULXs per early-type galaxy, and -0.15 ± 0.13 ULXs per elliptical galaxy. The ratio is then 0.03 ± 0.15 if we consider early-type galaxies, and -0.21 ± 0.19 if we consider ellipticals. The ratio for early-types can be taken as an upper limit on the fraction of Population II ULXs in spirals, since the old population of early-type/elliptical galaxies of the Liu

ULXs in spiral galaxies is small for any of these estimates, we neglect their contribution to our ULX sample.

B6 References and details for the single galaxies

Here we give the detailed references for the data used to compile Table 1, grouped by galaxy.

The Cartwheel (ESO 350-G 040): average SFR from Appleton & Marston (1997, H α data) and from Mayya et al. (2005, radio measurement); Z from Fosbury & Hawarden (1977), spectra of HII regions in the outer ring; X-ray sources from Wolter & Trinchieri (2004). This galaxy is not in the LB05 catalogue. Distance from the NASA Extragalactic Database (hereafter NED), assuming $H_0 = 73 \text{ km s}^{-1} \text{ Mpc}^{-1}$ and $V(\text{LocalGroup}) = 9048 \text{ km s}^{-1}$. Angular size and axis ratio from the RC3 catalogue; N_H from DL90.

NGC 253: SFR from Grimm, Gilfanov & Sunyaev (2003); Z from Webster & Smith (1983), that reports the measurements of line intensities for OII[$\lambda 3727 + \lambda 3729$] and OIII[$\lambda 4959 + \lambda 5007$], from which we derive the metallicity with the formula by P01; X-ray from LM05.

NGC 300: SFR from Helou et al. (2004), H α measurement, using the correlation by K98; metallicity gradient from PVC04; X-ray from LB05.

NGC 598 (M 33): SFR from ultra-violet (Muñoz-Mateos et al. 2007); metallicity gradient from spectra of HII regions (PVC04); X-ray from LM05. This galaxy is not in the LB05 catalogue. Distance from NED (mean redshift-independent distance). Angular size and axis ratio from the RC3 catalogue; N_H from DL90.

NGC 628 (M 74): SFR from Grimm et al. (2003); metallicity gradient from spectra of HII regions (Pilyugin et al. 2002); X-ray from LM05. This galaxy is not in the LB05 catalogue. Distance from NED (mean redshift-independent distance). Angular size and axis ratio from the RC3 catalogue; N_H from DL90.

NGC 1058: SFR from H α (Kennicutt & Kent 1983), using the correlation by K98; metallicity gradient from Moustakas & Kennicutt (2006a), based on the PT05 calibration; X-ray from LM05. This galaxy is not in the LB05 catalogue. Distance from NED (mean redshift-independent distance). Angular size and axis ratio from the RC3 catalogue; N_H from DL90.

NGC 1073: SFR from H α (Martin & Friedli 1997), using the correlation by K98; metallicity gradient from spectra of HII regions (Dors & Copetti 2005); X-ray from LB05.

NGC 1291: SFR from ultra-violet (Muñoz-Mateos et al. 2007); Z from X-ray measurements (Irwin, Sarazin & Bregman 2002); X-ray from LM05.

NGC 1313: SFR from H α (Ryder & Dopita 1994); Z from spectra of HII regions (P01); X-ray from Colbert et al. (1995).

NGC 1365: average SFR from mid- and far-infrared measurements (Lonsdale & Helou 1985; Strateva & Komossa 2009a, 2009b); metallicity gradient from spectra of HII regions (PVC04); X-ray from Strateva & Komossa (2009a).

et al.(2006) sample is typically larger than the old population in the spiral/irregular galaxies of the same sample.

IC 342 (PGC 13826): SFR from Grimm et al. (2003); metallicity gradient from spectra of HII regions (PVC04); X-ray from LM05.

NGC 1566: SFR from far-infrared ($\text{SFR}_{\text{FIR}} = 3.24 \text{ M}_{\odot} \text{ yr}^{-1}$, Bell & Kennicutt 2001, using the correlation by K98); Z from spectra of HII regions (Hawley & Phillips 1980); X-ray from LB05.

NGC 1705: average SFR from two different H α measurements ($\text{SFR}_{\text{H}\alpha} = 0.063 \text{ M}_{\odot} \text{ yr}^{-1}$, Gil de Paz, Madore & Pevunova 2003; $\text{SFR}_{\text{H}\alpha} = 0.112 \text{ M}_{\odot} \text{ yr}^{-1}$, Hunter & Elmegreen 2004), using the correlation by K98; Z from Lee & Skillman (2004), spectra of HII regions; X-ray from LB05.

NGC 2366: average SFR from H α ($\text{SFR}_{\text{H}\alpha} = 0.125 \text{ M}_{\odot} \text{ yr}^{-1}$, Hunter & Elmegreen 2004, using the calibration by K98, 8–1000 μm ($\text{SFR}_{\text{IR}} = 0.03 \text{ M}_{\odot} \text{ yr}^{-1}$, Hopkins, Schulte-Ladbeck & Drozdovsky 2002, using the calibration by K98 and radio ($\text{SFR}_{1.4\text{GHz}} = 0.069 \text{ M}_{\odot} \text{ yr}^{-1}$, Condon, Cotton & Broderick 2002, using the calibration by Bell 2003); Z from spectra of HII regions (PVC04); X-ray from LB05.

NGC 2403: SFR from Gilfanov, Grimm & Sunyaev (2004a); metallicity gradient from spectra of HII regions (PVC04); X-ray from LM05.

NGC 2442: average SFR from ultra-violet ($\text{SFR}_{\text{UV}} = 3.86 \text{ M}_{\odot} \text{ yr}^{-1}$, Muñoz-Mateos et al. 2007) and H α ($\text{SFR}_{\text{H}\alpha} = 5.26 \text{ M}_{\odot} \text{ yr}^{-1}$, Helmboldt et al. 2004, using the calibration by K98); metallicity gradient from spectra of HII regions (PVC04); X-ray from LB05.

Holmberg II (Arp 268, PGC 23324): SFR from H α (Walter et al. 2007), adopting the relation in K98; Z from spectra of HII regions (Walter et al. 2007); X-ray from Dewangan et al. (2004).

NGC 2903: average SFR from far-infrared ($\text{SFR}_{\text{FIR}} = 1.8 \text{ M}_{\odot} \text{ yr}^{-1}$, Ranalli et al. 2003, using the calibration by K98; $\text{SFR}_{\text{FIR}} = 1.5 \text{ M}_{\odot} \text{ yr}^{-1}$, Bell 2003, using the calibration by K98) and radio ($\text{SFR}_{1.4\text{GHz}} = 2.6 \text{ M}_{\odot} \text{ yr}^{-1}$, Ranalli et al. 2003, using the calibration by Bell 2003; $\text{SFR}_{1.4\text{GHz}} = 1.6 \text{ M}_{\odot} \text{ yr}^{-1}$, Bell 2003); metallicity gradient from spectra of HII regions (Pilyugin, Thuan & Vílchez 2006); X-ray from LB05.

NGC 3031 (M 81): SFR from ultra-violet (Muñoz-Mateos et al. 2007); metallicity gradient from spectra of HII regions (PVC04); X-ray from LM05.

NGC 3049: SFR from radio (Bell 2003); average Z from Guseva, Izotov & Thuan (2000) and Kehrig, Telles & Cuisinier (2004); X-ray from LB05.

PGC 30819 (IC 2574, UGC 05666): average SFR from H α ($\text{SFR}_{\text{H}\alpha} = 0.076 \text{ M}_{\odot} \text{ yr}^{-1}$, Miller & Hodge 1994, using the calibration by K98) and radio ($\text{SFR}_{1.4\text{GHz}} = 0.039 \text{ M}_{\odot} \text{ yr}^{-1}$, Condon et al. 2002, using the calibration by Bell 2003); Z from spectra of HII regions (Miller & Hodge 1996); X-ray from LB05.

NGC 3310 (Arp 217): SFR from Grimm et al. (2003); Z from spectra of HII regions (Pastoriza et al. 1993), metallicity from spectra of HII regions; X-ray from LM05.

NGC 3395/3396 (Arp 270): SFR from radio (Condon et al. 2002), using the calibration by Bell (2003); Z from integrated spectrum (Kennicutt 1992); X-ray from Brassington et al. (2005).

PGC 35286 (UGC 06456): SFR from H α (Hunter & Elmegreen 2004), using the calibration by K98; Z from spectra of HII regions (Pilyugin 2001b); X-ray from LB05.

PGC 35684 (UGC 06541, Mkn 178): SFR from H α (Hunter & Elmegreen 2004), using the calibration by K98; Z from spectra of HII regions (Pilyugin 2001b); X-ray from LB05.

NGC 3738 (Arp 234): average SFR from H α ($\text{SFR}_{\text{H}\alpha} = 0.047 \text{ M}_{\odot} \text{ yr}^{-1}$, Hunter & Elmegreen 2004) and radio ($\text{SFR}_{1.4\text{GHz}} = 0.029 \text{ M}_{\odot} \text{ yr}^{-1}$, Condon et al. 2002, using the calibration by Bell 2003); Z from spectra of HII regions (Martin 1997); X-ray from LB05.

NGC 3972: average SFR from H α ($\text{SFR}_{\text{H}\alpha} = 0.15 \text{ M}_{\odot} \text{ yr}^{-1}$, Moustakas & Kennicutt 2006b, using the calibration by K98), far-infrared ($\text{SFR}_{\text{FIR}} = 0.38 \text{ M}_{\odot} \text{ yr}^{-1}$, Bell 2003, using the calibration by K98) and radio ($\text{SFR}_{1.4\text{GHz}} = 0.36 \text{ M}_{\odot} \text{ yr}^{-1}$, Bell 2003); Z from spectra of HII regions (PT05); X-ray from LB05.

The Antennae (NGC 4038/4039, Arp 244): SFR from Grimm et al. (2003); X-ray estimate of Z (Fabbiano et al. 2004); X-ray from Fabbiano, Zezas & Murray (2001), spectral fits from LM05. The *Chandra* observation was analyzed only in a central area of $\sim 5.9 \text{ arcmin}^2$. This galaxy is not in the LB05 catalogue. Distance from NED (mean redshift-independent distance). Angular sizes and axis ratios from the RC3 catalogue; N_{H} from DL90.

NGC 4144: average SFR from H α ($\text{SFR}_{\text{H}\alpha} = 0.05 \text{ M}_{\odot} \text{ yr}^{-1}$, Moustakas & Kennicutt 2006b, using the calibration by K98) and radio ($\text{SFR}_{1.4\text{GHz}} = 0.05 \text{ M}_{\odot} \text{ yr}^{-1}$, Condon et al. 2002, with the calibration by Bell 2003); Z from spectra of HII regions (PT05); X-ray from LB05.

NGC 4214: average SFR from H α ($\text{SFR}_{\text{H}\alpha} = 0.18 \text{ M}_{\odot} \text{ yr}^{-1}$, Hunter & Elmegreen 2004; $\text{SFR}_{\text{H}\alpha} = 0.10 \text{ M}_{\odot} \text{ yr}^{-1}$, Schmitt et al. 2006, using the calibration by K98), far-infrared ($\text{SFR}_{\text{FIR}} = 0.15 \text{ M}_{\odot} \text{ yr}^{-1}$, Bell 2003; $\text{SFR}_{\text{FIR}} = 0.11 \text{ M}_{\odot} \text{ yr}^{-1}$, Schmitt et al. 2006, using the calibration by K98) and radio ($\text{SFR}_{1.4\text{GHz}} = 0.13 \text{ M}_{\odot} \text{ yr}^{-1}$, Bell 2003); Z from spectra of HII regions (PT05); X-ray from LB05.

NGC 4236: SFR from radio (Condon et al. 2002, using the calibration by Bell 2003); Z from spectra of HII regions (Vigroux, Stasińska & Comte 1987); X-ray from LB05.

NGC 4248: SFR from Moustakas & Kennicutt (2006b); Z from spectra of HII regions (PT05); X-ray from LB05.

NGC 4254 (M 99): average SFR from H α ($\text{SFR}_{\text{H}\alpha} = 3.9 \text{ M}_{\odot} \text{ yr}^{-1}$, Kennicutt, Tamblyn & Congdon 1994; $\text{SFR}_{\text{H}\alpha} = 5.4 \text{ M}_{\odot} \text{ yr}^{-1}$, Buat et al. 2002; $\text{SFR}_{\text{H}\alpha} = 3.2 \text{ M}_{\odot} \text{ yr}^{-1}$, Moustakas & Kennicutt 2006b) and far-infrared ($\text{SFR}_{\text{FIR}} = 3.48 \text{ M}_{\odot} \text{ yr}^{-1}$, Buat et al. 2002); metallicity gradient from spectra of HII regions (Moustakas & Kennicutt 2006a); X-ray from LB05.

NGC 4258 (M 106): SFR from radio (Condon et al. 2002, using the calibration by Bell 2003); metallicity gradient from spectra of HII regions (PVC04); X-ray from LB05.

NGC 4303 (M 61): average SFR from ultra-violet ($\text{SFR}_{\text{UV}} = 8 \text{ M}_{\odot} \text{ yr}^{-1}$, Muñoz-Mateos et al. 2007) and from H α ($\text{SFR}_{\text{H}\alpha} = 3.6 \text{ M}_{\odot} \text{ yr}^{-1}$, Moustakas & Kennicutt 2006b); metallicity gradient from spectra of HII regions (Moustakas & Kennicutt 2006a); X-ray from LB05 and from Tschöke, Hensler & Junkes (2000), whose sources B and F are not present in LB05.

NGC 4321 (M 100): SFR from Grimm et al. (2003); metallicity gradient from spectra of HII regions (Moustakas

& Kennicutt 2006a); X-ray from Kaaret (2001) and from LB05.

NGC 4395: SFR from ultra-violet (Muñoz-Mateos et al. 2007); metallicity gradient from spectra of HII regions (PVC04); X-ray from LM05.

NGC 4449: average SFR from far-infrared ($\text{SFR}_{\text{FIR}} = 0.22 \text{ M}_{\odot} \text{ yr}^{-1}$, Bell 2003; $\text{SFR}_{\text{FIR}} = 0.21 \text{ M}_{\odot} \text{ yr}^{-1}$, Ranalli et al. 2003, using the calibration by K98) and radio ($\text{SFR}_{1.4\text{GHz}} = 0.42 \text{ M}_{\odot} \text{ yr}^{-1}$, Bell 2003); Z from spectra of HII regions (Skillman, Kennicutt & Hodge 1989); X-ray from LB05.

NGC 4485/4490 (Arp 269): average SFR from H α ($\text{SFR}_{\text{H}\alpha} = 5.49 \text{ M}_{\odot} \text{ yr}^{-1}$, Kennicutt et al. 1987, assuming the calibration by K98 and an extinction of $\sim 1 \text{ mag}$, Clemens, Alexander & Green 1999); metallicity gradient from spectra of HII regions (Pilyugin & Thuan 2007); X-ray from LM05.

NGC 4501 (M 88): SFR from radio measurements by Condon et al. (2002); other measurements indicate both lower values ($1.4 \text{ M}_{\odot} \text{ yr}^{-1}$, from H α photometry reported in Gavazzi et al. 2002), and higher values ($6.0 \text{ M}_{\odot} \text{ yr}^{-1}$, from FIR measurements reported in Spinoglio et al. 2002); metallicity gradient from spectra of HII regions (Pilyugin et al. 2002); X-ray from LM05.

NGC 4559: SFR from radio (Condon et al. 2002), using the calibration by Bell (2003); metallicity gradient from spectra of HII regions (PVC04); X-ray from Cropper et al. (2004).

NGC 4631 (Arp 281): SFR from far-infrared (Ranalli et al. 2003, using the correlation by K98); Z from spectra of HII regions (Pilyugin, Izotova & Sholudchenko 2008); X-ray from LM05.

NGC 4651 (Arp 189): average SFR from H α ($\text{SFR}_{\text{H}\alpha} = 1.2 \text{ M}_{\odot} \text{ yr}^{-1}$, Hirashita et al. 2003, using the correlation by K98), far-infrared ($\text{SFR}_{\text{FIR}} = 1.6 \text{ M}_{\odot} \text{ yr}^{-1}$, Bell 2003, using the calibration by K98) and radio ($\text{SFR}_{1.4\text{GHz}} = 1.3 \text{ M}_{\odot} \text{ yr}^{-1}$, Bell 2003); metallicity gradient from spectra of HII regions (Moustakas & Kennicutt 2006a); X-ray from LB05.

NGC 4656: average SFR from H α ($\text{SFR}_{\text{H}\alpha} = 0.54 \text{ M}_{\odot} \text{ yr}^{-1}$, Moustakas & Kennicutt 2006b) and radio ($\text{SFR}_{1.4\text{GHz}} = 1.35 \text{ M}_{\odot} \text{ yr}^{-1}$, Condon et al. 2002, using the calibration by Bell 2003); Z from spectra of HII regions (Pilyugin, Izotova & Sholudchenko 2008); X-ray from LB05.

The Mice (NGC 4676, Arp 242): SFR from far-infrared (Brassington, Ponman & Read 2007, using the correlation by K98); X-ray estimate of Z (Read 2003); X-ray from Read (2003); but these observations are complete only for objects with $L_{\text{X}} \gtrsim 3 \times 10^{39} \text{ erg s}^{-1}$; so, it is quite likely that the actual number of ULX is larger than what we report in Table 1 (6). This galaxy is not in the LB05 catalogue. Distance from NED (assuming $H_0 = 73 \text{ km s}^{-1} \text{ Mpc}^{-1}$ and $V(\text{LocalGroup}) = 6602 \text{ km s}^{-1}$). Angular sizes and axis ratios from the RC3 catalogue; N_{H} from DL90.

NGC 4736 (M 94): SFR from Grimm et al. (2003); metallicity gradient from Moustakas & Kennicutt (2006a); X-ray from LB05.

NGC 4861 (Arp 266): SFR from H α (Schmitt et al. 2006), adopting the relation in K98; Z from spectra of HII regions (Izotov, Thuan & Lipovetsky 1997); X-ray from LM05.

PGC 45561 (UGC 08231): SFR from $H\alpha$ (Kewley et al. 2002), adopting the relation in K98; Z from spectra of HII regions (Kewley, Jansen & Geller 2005); X-ray from LB05.

NGC 5033: SFR from $H\alpha$ (Kennicutt & Kent 1983), using the correlation by K98; metallicity gradient from spectra of HII regions (PVC04); X-ray from LM05.

NGC 5055 (M 63): SFR from radio (Bell 2003); metallicity gradient from spectra of HII regions (PVC04); X-ray from LM05.

NGC 5194/5195 (M 51, Arp 85): SFR from ultra-violet (Muñoz-Mateos et al. 2007); metallicity gradient from spectra of HII regions with T_e method (PT05); X-ray from LM05.

NGC 5236 (M 83): SFR from Grimm et al. (2003); metallicity gradient from spectra of HII regions (Pilyugin et al. 2006); X-ray from LM05.

NGC 5238 (Mkn 1479): SFR from $H\alpha$ (Moustakas & Kennicutt 2006b); Z from spectra of HII regions (Moustakas & Kennicutt 2006a); X-ray from LB05.

NGC 5408: SFR from far-infrared (Stevens, Forbes & Norris 2002), adopting the correlation between SFR and FIR in K98; Z from spectra of HII regions (Masegosa, Moles & Campos-Aguilar 1994); X-ray from LM05. This galaxy is not in the LB05 catalogue. Distance from NED (mean redshift-independent distance). Angular size and axis ratio from the RC3 catalogue; N_H from DL90.

NGC 5457 (M 101, Arp 26): average SFR from ultra-violet ($SFR_{UV} = 5.05 M_\odot \text{ yr}^{-1}$, Bell & Kennicutt 2001; Muñoz-Mateos et al. 2007), $H\alpha$ ($SFR_{H\alpha} = 2.58 M_\odot \text{ yr}^{-1}$, Kennicutt et al. 1994; Bell & Kennicutt 2001) and radio ($SFR_{1.4\text{GHz}} = 2.02 M_\odot \text{ yr}^{-1}$, Condon et al. 2002; Bell 2003; Ranalli et al. 2003); metallicity gradient from spectra of HII regions (Pilyugin & Thuan 2007); X-ray from LM05.

Circinus (PGC 50779): SFR from Grimm et al. (2003); estimate of Z from optical lines (Oliva, Marconi & Moorwood 1999), in agreement with an X-ray estimate of Z (Smith & Wilson 2001). The measurement of Z might be affected by the central AGN; X-ray from LM05. This galaxy is not in the LB05 catalogue. Distance from NED (mean redshift-independent distance). Angular size and axis ratio from the RC3 catalogue; N_H from DL90.

NGC 6946 (Arp 29): SFR from radio (Bell 2003); metallicity gradient from spectra of HII regions (Pilyugin et al. 2002); X-ray from LM05.

PGC 68618 (IC 5201): SFR from $H\alpha$ (Dopita & Ryder 1994; Ryder & Dopita 1994), adopting the relation in K98; metallicity gradient from spectra of HII regions (PVC04); X-ray from LB05.

NGC 7714/7715 (Arp 284, Mkn 538): SFR from far-infrared (Schmitt et al. 2006), adopting the relation in K98; Z from spectra of HII regions (Gonzalez-Delgado et al. 1995); X-ray from Smith, Struck & Nowak (2005).

NGC 7742: average SFR from ultra-violet ($SFR_{UV} = 1.00 M_\odot \text{ yr}^{-1}$, Iglesias-Páramo et al. 2006), $H\alpha$ ($SFR_{H\alpha} = 1.40 M_\odot \text{ yr}^{-1}$, Trinchieri, Fabbiano & Bandiera 1989) and FIR ($SFR_{FIR} = 1.42 M_\odot \text{ yr}^{-1}$, Trinchieri et al. 1989); Z from spectra of HII regions (PT05); X-ray from LB05.

Milky Way (MW): SFR from Grimm et al. (2003); metallicity gradient ($Z(r) = 8.762 - 0.356r/R_{25}$) from OB stars (Daflon & Cunha 2004); X-ray from Grimm, Gilfanov

& Sunyaev (2002). This galaxy is not in the LB05 catalogue. Suggested IAU distance to MW centre. Angular size and N_H were not used.

IC 10: SFR reported in table 2 of Legrand et al. (2001); Z from spectra of HII regions (Garnett 1990), Z from spectra of HII regions; X-ray from Wang, Whitaker & Williams (2005). This galaxy is not in the LB05 catalogue. Distance from NED (mean redshift-independent distance). Angular size and axis ratio from the RC3 catalogue; N_H from DL90.

Large Magellanic Cloud (LMC): SFR from Grimm et al. (2003); metallicity gradient from spectra of HII regions (PVC04); X-ray from Long, Helfand & Grabelsky (1981). This galaxy is not in the LB05 catalogue. Distance from NED (mean redshift-independent distance). Angular size and N_H were not used.

Small Magellanic Cloud (SMC): SFR from Grimm et al. (2003); metallicity gradient from spectra of HII regions (PVC04); X-ray from Wang & Wu (1992). This galaxy is not in the LB05 catalogue. Distance from NED (mean redshift-independent distance). Angular size and N_H were not used.

APPENDIX C: ANALYSIS OF ϵ_{BH}

ϵ_{BH} is defined as the ratio between N_{ULX} and N_{BH} (see equation 4). Table C1 and Figs. C1 and C2 show that the behaviour of ϵ_{BH} as a function of the SFR and of the metallicity is consistent with a constant. This result supports the hypothesis that N_{BH} is proportional to N_{ULX} , although the error bars on ϵ_{BH} are very large.

We point out that the trend that can be seen in the left-hand panels of Figs. C1 and C2 (ϵ_{BH} versus SFR) is much less significant than it appears. In fact, in galaxies with a low SFR the presence of a single ULX can easily increase the value of ϵ_{BH} , populating the top-left part of the diagrams. We checked the importance of this effect by looking at the 23 galaxies with $SFR \leq 0.3 M_\odot \text{ yr}^{-1}$: the average of their ϵ_{BH} , weighted on N_{BH} , is $\sim (9 \pm 5) \times 10^{-4}$, in the P98 case. Such value is much more in line with the results for galaxies with higher SFR; it is still a bit higher than the average, but this might be due to some form of publication/observation bias.

Table C1. Parameters of the power-law fits and χ^2 for ϵ_{BH} .

x - axis	y - axis	Stellar evolution model	Index	Normalization	χ^2/dof ^a	r (p_r) ^b
SFR [$M_\odot \text{ yr}^{-1}$]	ϵ_{BH}	P98	-0.27 ± 0.19	$-3.02^{+0.09}_{-0.12}$	17.8/62	0.43 (5×10^{-4})
SFR [$M_\odot \text{ yr}^{-1}$]	ϵ_{BH}	P98	0.00	-3.18 ± 0.07	19.7/63	0.43 (5×10^{-4})
Z/Z_\odot	ϵ_{BH}	P98	$0.01^{+0.36}_{-0.27}$	$-3.17^{+0.27}_{-0.23}$	19.7/62	0.25 (5×10^{-2})
Z/Z_\odot	ϵ_{BH}	P98	0.00	-3.18 ± 0.07	19.7/63	0.25 (5×10^{-2})
SFR [$M_\odot \text{ yr}^{-1}$]	ϵ_{BH}	B10	-0.26 ± 0.19	$-3.27^{+0.10}_{-0.13}$	8.2/62	-0.06 (7×10^{-1})
SFR [$M_\odot \text{ yr}^{-1}$]	ϵ_{BH}	B10	0.00	-3.43 ± 0.06	10.0/63	-0.06 (7×10^{-1})
Z/Z_\odot	ϵ_{BH}	B10	-0.16 ± 0.29	-3.54 ± 0.22	9.6/62	-0.23 (7×10^{-2})
Z/Z_\odot	ϵ_{BH}	B10	0.00	-3.43 ± 0.06	10.0/63	-0.23 (7×10^{-2})

Notes. The sample adopted for the fit in this Table is represented by all the galaxies in Table 1. ^a χ^2/dof is the χ^2 divided by the degrees of freedom (dof). ^b r is the Pearson correlation coefficient, and p_r is the probability of finding a value larger than $|r|$, if the two variables were uncorrelated and normally distributed.

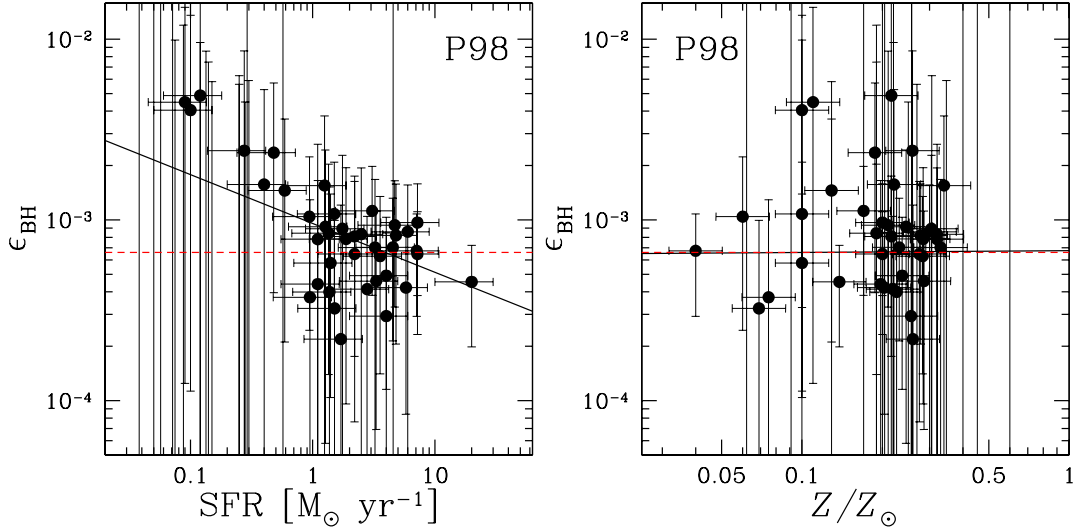


Figure C1. ϵ_{BH} as a function of the SFR (left-hand panel) and of Z (right-hand panel) for P98. The filled circles are the galaxies listed in Table 1. The error bars on both the x - and the y - axis are $1 - \sigma$ errors (see Section 2.3 for details). The solid lines are the power-law fits for the sample with $N_{\text{ULX}} > 0$. The dashed lines (red on the web) are fits with a constant value for the same sample.

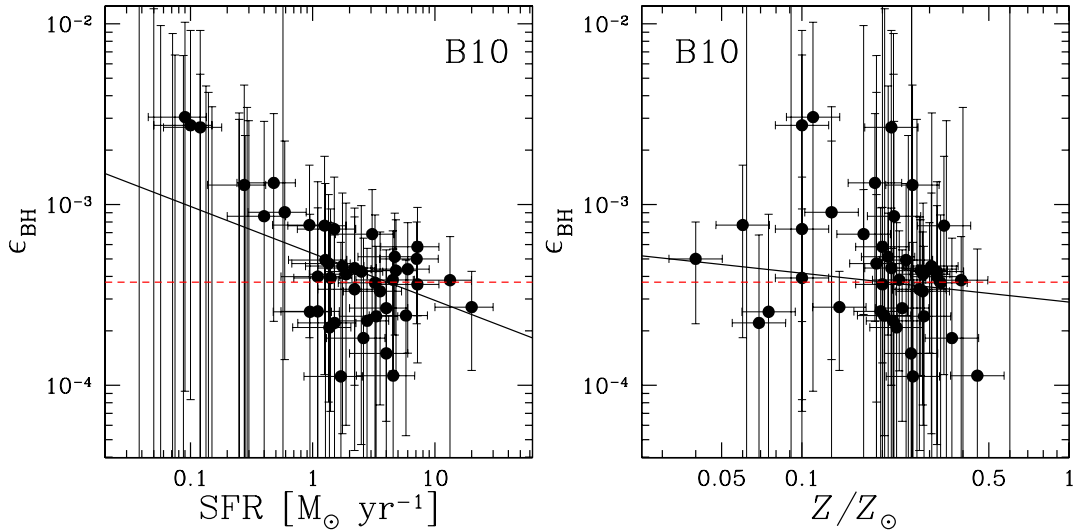


Figure C2. The same as Fig. C1 for B10.